COMPARATIVE ASSESSMENT OF THE SEISMIC PERFORMANCE OF FIXED BASE AND ROCKING BUILDING FRAMES EQUIPPED WITH AN ENERGY DISSIPATION SYSTEM

A THESIS SUBMITTED TO
THE GRADUATE SCHOOL OF NATURAL AND APPLIED SCIENCES
OF
MIDDLE EAST TECHNICAL UNIVERSITY

BY

HAZAL ÖZEN

IN PARTIAL FULFILLMENT OF THE REQUIREMENTS
FOR
THE DEGREE OF MASTER OF SCIENCE
IN
ENGINEERING SCIENCES

MARCH 2023

Approval of the thesis:

COMPARATIVE ASSESSMENT OF THE SEISMIC PERFORMANCE OF FIXED BASE AND ROCKING BUILDING FRAMES EQUIPPED WITH AN ENERGY DISSIPATION SYSTEM

submitted by **HAZAL ÖZEN** in partial fulfillment of the requirements for the degree of **Master of Science in Engineering Sciences Department, Middle East Technical University** by,

Prof. Dr. Halil Kalıpçılar
Dean, Graduate School of **Natural and Applied Sciences** _____

Prof. Dr. Murat Dicleli
Head of Department, **Engineering Sciences** _____

Prof. Dr. Murat Dicleli
Supervisor, **Engineering Sciences, METU** _____

Examining Committee Members:

Prof. Dr. Tolga Akış
Civil Engineering, Atılım University _____

Prof. Dr. Murat Dicleli
Engineering Sciences, METU _____

Assoc. Prof. Dr. Zehra Çağnan Ertuğrul
Engineering Sciences, METU _____

06.03.2023

I hereby declare that all information in this document has been obtained and presented in accordance with academic rules and ethical conduct. I also declare that, as required by these rules and conduct, I have fully cited and referenced all material and results that are not original to this work.

Name, Surname: Hazal Özen

Signature :

ABSTRACT

COMPARATIVE ASSESSMENT OF THE SEISMIC PERFORMANCE OF FIXED BASE AND ROCKING BUILDING FRAMES EQUIPPED WITH AN ENERGY DISSIPATION SYSTEM

Özen, Hazal
M.S., Department of Engineering Sciences
Supervisor: Prof. Dr. Murat Dicleli

March 2023, 83 pages

In this study, the effect of columns with a rocking-base isolation system on enhancing the seismic performance of a reinforced concrete building is investigated. A comparative study comprising of comparisons of fixed-based and rocking-based systems with post-tensioning strands and free column ends is conducted. For analysis purposes, a reinforced-concrete building with shear walls was designed, modeled, and analyzed in ETABS software. Nonlinear boundary time history analysis (NTHA) was conducted by exposing the structure to a set of ground motions scaled by taking reference from the California region in the USA. The effect of different parameters of the designed building was considered in the study such as a) the story height b) the number of bays c) the presence of shear walls d) the addition of dampers and different damping parameters. In addition, the NTHA was repeated for different ground motion intensity levels.

Keywords: Rocking Column, Seismic Base Isolation, Energy-dissipation, Parametric Study

ÖZ

ANKASTRE MESNETLİ VE ENERJİ EMME SİSTEMLERİYLE DONATILMIŞ SALINIM YAPAN BİNA ÇERÇEVELERİNİN KARŞILAŞTIRMALI OLARAK DEPREM PERFORMANSININ DEĞERLENDİRİLMESİ

Özen, Hazal
Yüksek Lisans, Mühendislik Bilimleri Bölümü
Tez Yöneticisi: Prof. Dr. Murat Dicleli

Mart 2023 , 83 sayfa

Bu çalışmada, betonarme yapının sismik performansının arttırılmasında, sallanan tabanlı izolasyon sistemli kolonların etkisi araştırılmıştır. Ard germe şeritleri ve serbest kolon uçları ile sabit tabanlı ve sallanan tabanlı sistemlerden oluşan karşılaştırmalı bir çalışma yürütülmüştür. Analiz amacıyla, perde duvarlı betonarme bir bina tasarlanmış, modellenmiş ve ETABS yazılımında analiz edilmiştir. Doğrusal olmayan sınır zaman alanı analizi (NTHA), yapı, ABD'deki California bölgesinden referans alınarak ölçeklendirilmiş bir dizi yer hareketine maruz bırakılarak yapılmıştır. Çalışmada tasarlanan yapının a) kat yüksekliği b) açıklık sayısı c) perde duvar varlığı d) damper varlığı gibi farklı parametrelerinin etkisi dikkate alınmıştır. Ayrıca, doğrusal olmayan sınır zaman alanı analizi farklı yer hareketi yoğunluk seviyeleri için tekrarlanmıştır.

Anahtar Kelimeler: Kolon Salınımı, Sismik İzolasyon, Enerji Sönümleme, Parametrik Çalışma

Dedicated in memory of my dear grandmother, Türkan Ödün.

ACKNOWLEDGMENTS

I wish to express my deepest gratitude to my supervisor Prof. Dr. Murat Dicleli for his guidance, advice, criticism, encouragement, and insight throughout the research. This study was completed thanks to his valuable knowledge on the subject, years of academic experience, and unique approach to problems that we encountered.

I would like to express my gratitude to Prof. Dr. Özgür Kurç and my colleagues at LARSA Eurasia for their knowledge, and support, and for providing an excellent working environment, enabling me to complete my work efficiently.

I want to express my thanks to my dearest friends, Sevda Rafatova, Ali Fatih Kuloğlu, Selen Ecem Oksay, Kübra Altınok, Gizem Buldu, Cansın Erkuş, Gül Özkuzukıran, and Cansu Aksu for their impeccable support and friendship throughout this journey. I wouldn't have found the strength to complete my studies without their support.

I would finally like to thank my dear family, especially my dear mother, Tülin Ödün, who has supported me immensely through this journey when things were extremely challenging. My brother Kazım Kutalp Yavuz, and sister Yasemin Meriç, who believed in me and always showed me their love and support. And last but not least, my dear father Mehmet Özen. Including my extended family members, I would not get through this time period if it wasn't for my family.

TABLE OF CONTENTS

LIST OF TABLES

TABLES

LIST OF FIGURES

FIGURES

LIST OF ABBREVIATIONS

2D	2 Dimensional
3D	3 Dimensional
NTHA	Nonlinear Time History Analysis
FRB	Free Rocking Base

CHAPTER 1

INTRODUCTION

In many highly populated countries and regions around the world, earthquakes are one of the most common natural disasters. The earthquake design provisions mainly concentrate on the prevention of collapse and ensuring life safety. Nevertheless, in order to increase safety, limit the economic losses due to seismic damage, and maintain building downtime, seismic isolation/energy dissipation systems come into the picture.

To acquire earthquake resilience in the structure, many different mechanisms were developed. As an alternative to the conventional seismic design that fixes the structure to the ground, two new seismic design concepts have been developed over the last fifty years in the context of the so-called "softening systems". One is base isolation, and the other is the concept of rocking structures. In seismic base isolation, the foundation system includes a very flexible layer that allows for large lateral displacements of the superstructure while sustaining the gravitational loads. In contrast, rocking systems allow the structure to uplift from the ground and rock.[3]

In the last few decades, researchers have been interested in rocking structures' performance. It was Housner who first introduced the effect of rocking motion on seismic energy dissipation by examining a rocking rigid body supported by a horizontally accelerated base. Housner observed that during May 1960 Chilean earthquakes, inverted pendulum structures with questionable stability survived the ground shaking with almost no damage. Whereas the reinforced concrete, elevated water tanks which appeared much more stable were severely damaged. The same applied to some tall, slender petroleum towers during the Arvin-Tehachapi earthquake in California in 1952, which rocked back and forth by stretching their anchor bolts and survived the

earthquake. In this study, Housner also examined the scale effect and concluded that the larger of the two geometrically similar blocks is more stable than the smaller one. Another conclusion of his study was that out of two identical acceleration amplitude pulses the one which has a longer duration is more likely to cause better stability. By allowing the rocking motion of the structure, it is expected that the structure's flexibility increases. Thus, the overall damage due to base excitation is reduced.
Later on, many other researchers expanded Housner's findings realizing the immense effect of the rocking motion on energy dissipation on structures subjected to ground excitation. For example, Cheng and Chao introduced rocking bearings that are still under moderate earthquakes but rock back and forth under severe excitation.[4] Some other researchers such as Chen et al, concentrated on self-centering rocking steel frame systems [5]. As for the reinforced concrete frames, Zhao and Su concentrated on a single-story, single-span prestressed concrete rocking frame's seismic performance.[6] E. Yooprasertchai and P. Warnitchai discuss the applicability of the combination of precast hybrid moment-resisting frames (PHMRFs) with precast concrete rocking walls (PCRWs) to achieve seismic resilience in buildings.

Even though there have been an increasing number of studies in each passing year regarding rocking base isolation, the careful literature research showed that none of these have comprehensively evaluated and compared the performance of rocking structures with various options such as comparisons of fixed base (I), free rocking base (II), free rocking base equipped with post-tensioning tendons (III), free rocking base + viscous fluid dampers (IV), free rocking base with post-tensioning tendons + viscous fluid dampers (V). In addition to these, the literature review showed that the number of stories and bays of the reinforced concrete frames, namely, the aspect ratio was another parameter that was not comprehensively examined for its effect on the rocking response of the frames where the current literature was shortcoming.

This study aims to prove the performance of rocking-based energy dissipation systems compared to the conventional fixed-based structures and propose a model for the rocking column systems in reinforced concrete frames and propose it as a useful tool for seismic energy absorption by taking into account the different options such as a) the story height b) the number of bays c) the presence of shear walls d) the addition of dampers and different damping parameters e) existence of PT tendons.

For the scope of this study, a reinforced concrete frame-shear wall system with planar symmetry was designed according to the ASCE 7-16 (Minimum Design Loads and Associated Criteria for Buildings and Other Structures) standards. The building is presumed to be located in the California region of the United States of America. For the design and analysis, ETABS software was used, which is a highly developed software for structural analysis and design of multi-story buildings. For the comparative assessment of the rocking-based energy dissipation system, a version of the model with a rocking outer column energy dissipation system with dampers was designed.

To simulate the ground motion, nonlinear time history analysis was conducted in the ETABS software. For this purpose, seven ground motion records were selected by filtering the ground motion records in the PEER (Pacific Earthquake Engineering Research) ground motion database. The design peak ground acceleration for this study is 0.5 g.

CHAPTER 2

LITERATURE REVIEW

The concept of rocking isolation was first introduced by Housner, in 1963, upon the performance of some tall slender water tanks in Chilean earthquakes. These water tanks were "golf-ball on a tee" types of structures, resembling inverted pendulums, and these structures survived the ground shaking whereas much more stable appearing reinforced-concrete elevated water tanks were severely damaged. Housner also concluded that there is a scale effect that makes tall slender structures more stable against overturning than might have been expected, and, therefore, the survival of such structures during earthquakes is not surprising [7].
Although Housner was the first to introduce rocking isolation to the modern structural engineering world, ancient builders have built structures with the same principle. Some of these structures have been standing for millennials such as the Temple of Aphaia in Aegina, Greece which is shown in Figure 2.1.

Its monolithic, free-standing columns support massive epistyles and the frieze atop. The entire rocking frame remains standing for more than 2500 years in a region with high seismicity mechanisms. The unparallel seismic performance of the rocking frames of Temple of Aphaia is due to the very reason that they are articulated mechanisms. In this way: (a) given their negative stiffnesses they are not subject to any resonance, (b) re-centering (elimination of any permanent displacement) is achieved unconditionally with gravity; and (c) the rocking frames, while slender and emblematic, they are large in size to the extent that their rotational inertia, when mobilized, is enough to resist the 2500 years seismic hazard [1].

Over the recent years, the attention of researchers on the rocking isolation of structures increased. Different methods for rocking isolation were introduced for both

Figure 2.1: Temple of Aphaia in Aegina, Greece which has been standing in a high seismicity region for more than 2500 years[1]

Reinforced-Concrete and Steel structures. For steel structures, one of these methods is the usage of weak base plates. In a study by Midorikawa et al, to cause rocking vibration under appropriate control, weak base plates are attached at the bottom of each steel column at the first story. When the weak base plates yield during a strong earthquake, the building causes rocking vibration [8]. In conclusion of this study, the rocking system with weak base plates was found to be effective to reduce the seismic responses of buildings.

Another method proposed for steel frames for rocking base isolation is self-centering bracing systems. Vertical post-tensioning tendons are designed to self-center the system after rocking, and energy dissipation may be provided to limit the peak displacements [9].

On the other hand for reinforced-concrete frames, similar methods for rocking base energy dissipation were introduced with post-tensioned strands, and uplift allowed column systems. G. Ríos-Garcíaa, A. Benavent-Climent proposed a new anchored rocking column that allows the slippage of the steel bar at the bottom end within a controlled range of displacements (gap). In comparison with conventional RC frames,

the proposed solution reduces the maximum inter-story drifts in the upper stories by about 3 times, the story accelerations about 1.5 times and the energy dissipation demand about 20 times [3].

Other alternatives, such as an Energy-Dissipative Rocking Column (EDRC) system for reinforced-concrete frames were introduced by researchers. The EDRC system is a combination of rocking components and metal energy-dissipative components. In this study, the results from the pseudo-dynamic tests showed that the maximum and residual inter-story drift ratio of EDRC-Frame system was reduced by 26.0% and 82.0%, respectively, comparing to MRF (Moment Resisting Frame). And the quasi-static test results showed that the ultimate capacity was increased by 27.0% comparing to MRF [10].

In another experimental study, the cyclic behavior of the rocking columns were examined. The numerical analysis results show that the use of rocking columns is an appropriate technique to achieve weakening and reducing the acceleration response. However, weakening alone is not sufficient if the displacement response exceeds a desirable limit. The addition of damping can correct this problem, making the system efficient for use in seismic areas [11].

In light of all these previous works a comparative study investigating the rocking energy dissipation on reinforced concrete frame-shear wall system was introduced. The aim is to study the benefit of rocking base isolated system compared to a fixed base system by also considering different control parameters such as number of stories, and number of bays, and different rocking base modeling methods.

CHAPTER 3

REVIEW OF THE ROCKING RESPONSE

Housner proposed a mathematical model for the rocking rigid body. The rigid body of which the free body diagram is shown in Figure 3.1, will oscillate about its centers of rotation O and O' when it undergoes rocking motion. The coefficient of friction is assumed to be large enough to ensure no sliding between the base and the rigid body. The significant properties of the rigid body are its weight denoted by W, its moment of inertia I is about the center of rotation O, and the location of its center of gravity. The radial distance of the center of gravity to the center of rotation is denoted by R. At rest, the block makes an alpha angle with the vertical. And the tilt angle from the vertical axis is measured by theta angle.

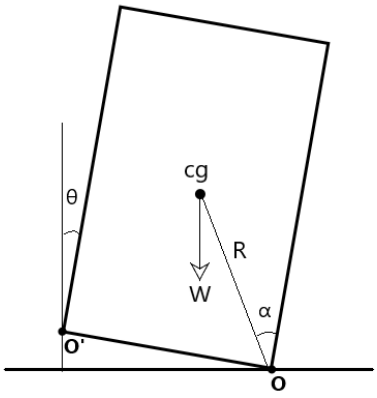

Figure 3.1: Free Body Diagram of the Rocking Body

The equation of motion of the rigid body experiencing time-dependent acceleration

a(t) is given below (Eqn. 3.1), where a(t) can represent any earthquake input. [12]

$$I\theta'' - MRa(\text{ø}tcos(\alpha \pm \theta) \pm MgRsin(\alpha \pm \theta) = 0 \tag{3.1}$$

M: Mass

I: Moment of inertia with respect to O or O' ($I = 4/3MR^2$)

R: Radial distance of the center of gravity of the rigid body to the point of rotation.

The plus minus sign represents the domains θ< 0 and θ> 0.

The computation of time-dependent acceleration a(τ) is given as follows (Eqn. 3.2).

$$a(\tau) = \alpha g \beta cos(\Omega\tau + \Phi) \tag{3.2}$$

The βand Ωvalues are respectively the earthquake amplitude and circular frequency.The remaining non-dimensional variables are introduced to be dx=θ/α, t=p τ, ω=Φ/p[12]

Where $p = \sqrt{MgR/I}$

g: gravitational acceleration.

After differentiating with respect to non dimensional time by Newton's notation, the eqution 3.1 becomes:

$$|\ddot{x}| + (1/\alpha)sin[\alpha(1 - |x|)] - sin(x)\beta cos[\alpha(1 - |x|)]cos(\omega t + \Phi) = 0 \tag{3.3}$$

Housner's piece-wise theory [7] assumes a coefficient of restitution which is multiplied by the angular velocity while the block is passing from equilibrium (x=0) Where $\dot{x}_1$ and $\dot{x}_2$ are the angular velocities of the rocking block, respectively, right before and right after the impact, the coefficient of restitution can be expressed as:

$$CR = \dot{x}_2/\dot{x}_1 \tag{3.4}$$

CR: Coefficient of Restitution

3.1 Impact

During the rocking motion, the column bases and the footing are colliding with each other which results in structural pounding. For this reason, a certain amount of impact damping and impact stiffness needs to be introduced to the system to improve the modeling of the controlled rocking columns. In order to simulate the impact, a point element is introduced at the point of contact which can mathematically described as a linear spring and dash-pot system.

For the calculation of impact damping and impact stiffness values, some other parameters need to be calculated. As previously denoted, the Coefficient of Restitution (CR) which is defined as the impact energy loss is the instantaneous kinetic energy reduction of the members at the moment of impact. The coefficient of Restitution calculation by Kalliontiz is given in Equation 3.5.[13]

$$CR = (\dot{\theta}_2/\dot{\theta}_1)^2 = [1 - \frac{MR^2}{I_o} \cdot (1 - cos2\alpha)]^2 \tag{3.5}$$

M: Equivalent mass of the two collapsing bodies.

R: Radial distance to the center of rotation.

$$c_{\text{imp}} = 2 \cdot \zeta \sqrt{k_s \frac{(m_1 \cdot m_2)}{(m_1 + m_2)}} \tag{3.6}$$

$$\zeta = -\frac{ln(CR)}{\sqrt{(\pi^2 + (ln(CR))^2)}} \tag{3.7}$$

m_1, m_2: Masses of the collapsing bodies.

ζ: Damping ratio.

k_s: equivalent stiffness of the collapsing bodies.

CHAPTER 4

DESCRIPTION OF THE BENCHMARK PROBLEM AND THE MODELING PROCEDURE

For the scope of this study, reinforced concrete frame-shear wall systems with different story heights were designed that are presumed to be located in the California region of the United States of America. The buildings designed for the parametric study have 4, 8,12, and 16-story levels. The buildings have plan symmetry in both horizontal X and Y axes. Each building has 5 bays which are each 6 meters in length. The story height is 3 meters at each story level measured from beam centroids. There is a core wall located at the center of the building and four symmetrical L-shaped shear walls are located at each corner.

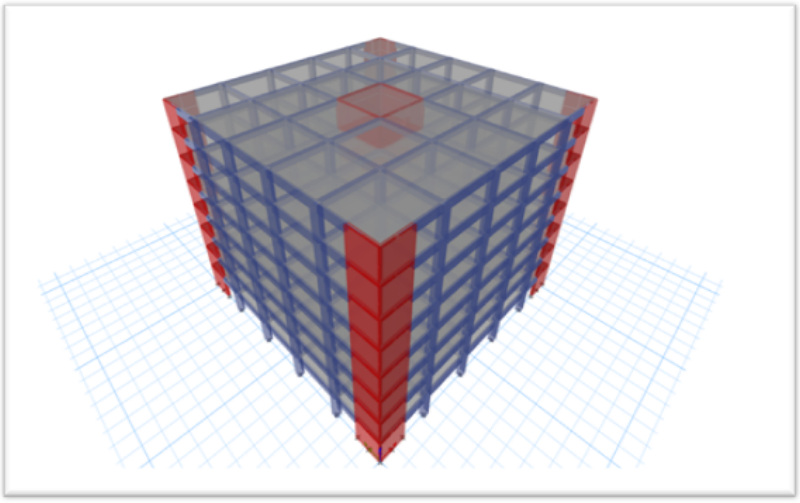

Figure 4.1: 3D View of the 8 Story Building ETABS

The benchmark model considered in the analysis is the 8-story 5-bay building model

shown in Figure 4.1. Later, for the sake of the comparative study, different versions of each building with different number of bays and outer columns free to rock are modeled as well. Different comparisons were carried out by taking different frames from the analyzed buildings narrowing the analysis down to a 2D System for simplicity and to avoid the analysis time cost. The analysis procedure and the comparison of the results are thoroughly covered in chapter 6.

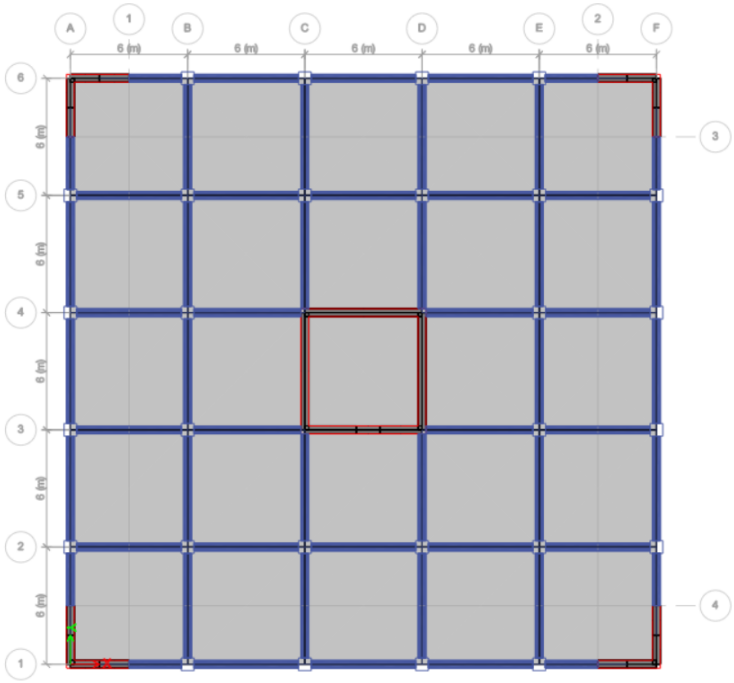

Figure 4.2: Plan view of the building

The design and modeling procedures of 8 story building will be explained in the following chapters.

4.1 Modeling Procedure

4.1.1 Description of the 3D Model

The building was modeled in ETABS, a software for structural analysis and design of multi-story buildings. 3D Modeling approach was chosen to be able to assess the effect of different structural parameters to the performance of the building with

rocking isolation under seismic loading.

The design of the 8-story, 5-bay reinforced concrete frame-shear wall system will be explained as a reference in this chapter. The bay width is 6 meters, and each story is 3 meters in height. At the corners, there are L-shaped shear walls. At the center of the building, there is an additional core shear wall. The L-shaped wall legs have a 3-meter length each, and the core dimensions are 6 m x 6 m.

The beams and the columns were modeled as 3D member elements whereas the shear walls were modeled with Thin-Shells. The floor slabs were modeled with Membrane type of elements to ensure the complete load transfer to the frame system and to eliminate its contribution of bending stiffness by plate action.

4.1.2 Loading

4.1.2.1 Dead Loads

Dead loads are the permanent loads acting on the structure. The material unit weights are automatically accounted for by the software.

- Unit weight of Concrete: 23.5642 kN/m3
- Unit weight of Steel: 76.9729 kN /m3

Additionally, uniform dead load was added to the floors due to the weight of non-structural components per ASCE 7-16 Table C3.1-1b Minimum Design Dead Loads.
Uniform Dead Load on Applied on Floors:

- Uniform Dead Load from Marble and mortar on stone–concrete fill = 1.58 kN/m².
- Uniform Dead Load on Ceiling level from Plaster = 0.25 kN/m²

Total Uniform Dead Load on Floors =1.83 kN/m²

Uniform Dead Load on Roof level:

- Clay Book tile, 51 mm +Mortar =1.15 kN/m²
- Plaster = 0.25 kN/m²

Total uniform dead load on roof = 1.40 kN/m²

Distributed Wall Load on Interior Beams:

- The wall load on interior walls was calculated by considering the unit weight of the walls as 40 lb / ft2 = 1.915 kN/m²

Story height-Beam depth = 2400 mm
Uniform wall load on interior beams = 1.915 kN/m² * 2.4 m= 4.6 kN/m
Distributed Wall Load on Exterior Beams:

- Clay Brick (12 inch) = 115 PSF = 5.506 kN/m²

Exterior stud walls:

- 2 × 4 @ 16-in., 58-in. gypsum, insulated, 38-in. siding = 11 PSF = 0.526 kN/m²
- Exterior stud walls with brick veneer (10 mm) = 48 psf = 2.298 kN/m²

Beam depth = 600 mm
Story Height = 3000 mm
Dead load on exterior wall = 2.824 kN/ m² * 2.4 m = 6.8 kN/m.

4.1.2.2 Live Loads

Live loads are the maximum expected loads for intended use or occupancy. From *ASCE 7-16 Table 4.3-1 Minimum Uniformly Distributed Live Loads, Lo, and Minimum Concentrated Live Loads:*

- Roof areas not intended for occupancy 20 lb/ft2 (0.96 kN/m²)
- Live Load on Floors = 40 lb/ft2 (1.915 kN/m²)

4.1.2.3 Seismic Load

Seismic Loads are the application of seismic oscillation to the structure. Seismic loading primarily depends on the seismic hazard, site geotechnical parameters, and the natural frequency of the structure.

In design, Response Spectra Load cases in X and Y directions were used to account for the seismic loading.*ASCE 7 Hazard Tool* was used to download a Response Spectra curve for the California region.

Table 4.1: Properties of the downloaded spectrum

Risk Category	II
Soil Class	C-Very Dense Soil and Soft Rock
Latitude, Longitude	37.85698, -121.523306
Elevation	-6.43 ft (NAVD 88)
PGA	0.53 g
S_{DS}	0.91
S_{D1}	0.37
T_L	8 s
V_{S30}	530 m/s

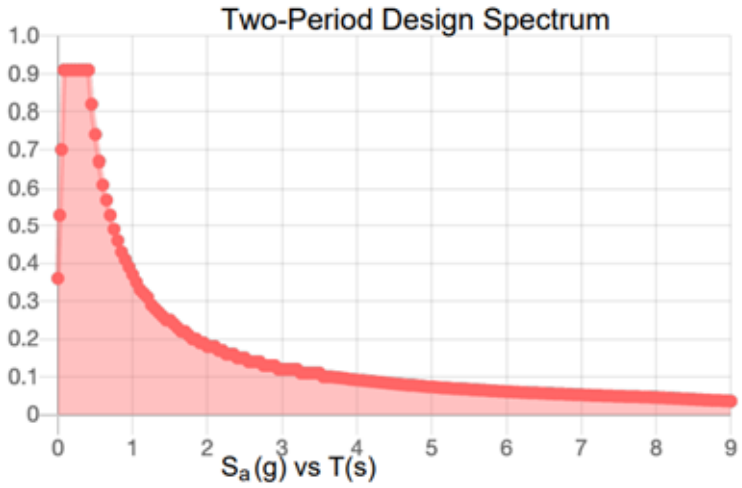

Figure 4.3: Selected Response Spectra Curve

This ground motion was scaled for 0.5 g and the scaled response spectrum curve was used for seismic loading in the design.

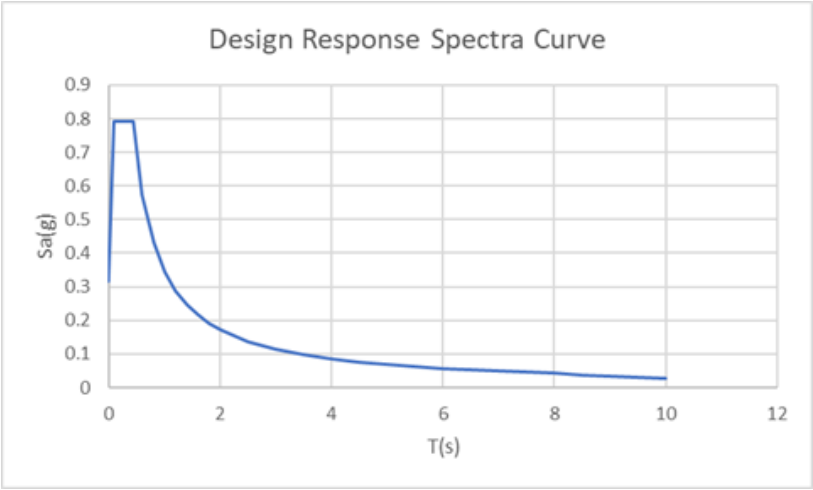

Figure 4.4: Scaled Design Response Spectra Curve

The design response spectrum curve was defined in ETABS

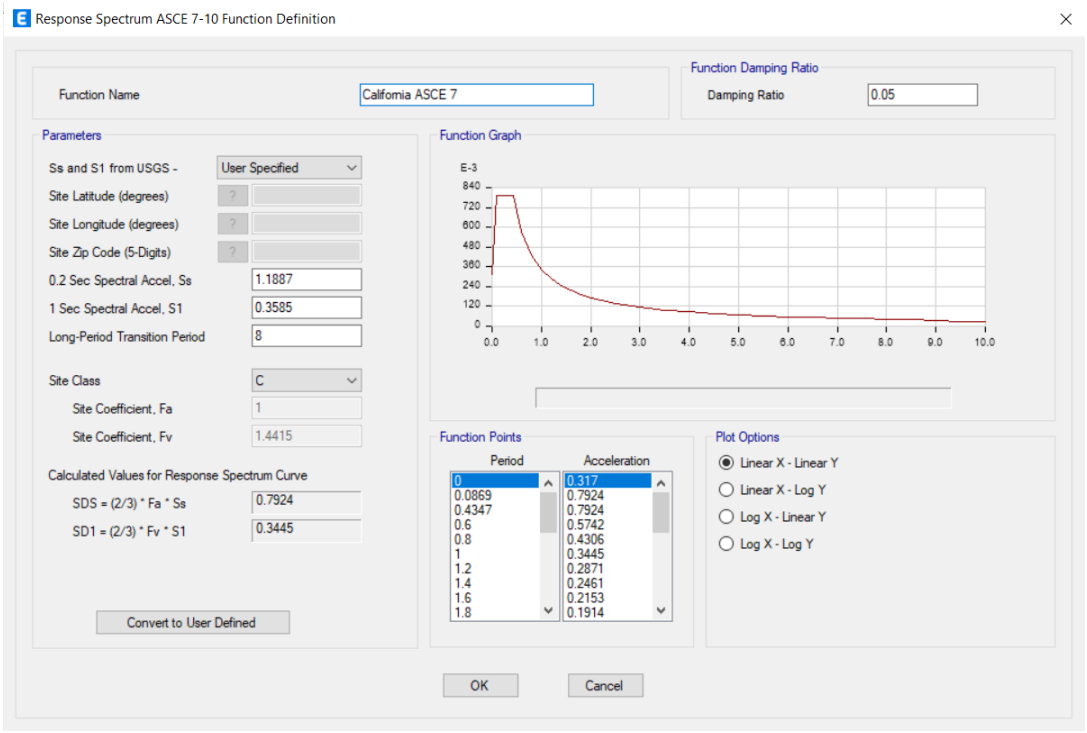

Figure 4.5: Response Spectrum Curve properties defined in ETABS software

4.1.2.4 Load Combinations for Design

The load combinations considered for design are the basic combinations from ASCE 7 Section 2.3-*Combining Factored Loads Using Strength Design.*

Table C2.3-1 Principal Loads for Strength Design Load Combinations

	Load Combination	Principal Load
1	$1.4D$	D
2	$1.2D + 1.6L + 0.5(L_r \text{ or } S \text{ or } R)$	L
3	$1.2D + 1.6(L_r \text{ or } S \text{ or } R) + (1.0L \text{ or } 0.5W)$	L_r or S or R
4	$1.2D + 1.0W + 1.0L + 0.5(L_r \text{ or } S \text{ or } R)$	W
5	$0.9D + 1.0W$	W
6	$1.2D + E_v + E_h + L + 0.2S$	E
7	$0.9D - E_v + E_h$	E

Figure 4.6: ASCE 7-16 Principal Load Combinations for Strength 14

Wind, Snow, and Rain loads are not included in this analysis. Therefore, the basic load combinations for design are reduced to:

1. 1.4 D
2. 1.2 D + 1.6 L
3. 1.2 D + E + L
4. 0.9 D + E

Per ASCE 7- 16 requirements, the directional and vertical effects of the seismic load were accounted for.

$$E = Eh + Ev$$

Eh: horizontal seismic load effect.

Ev: vertcal seismic load effect.

The vertical seismic load effect is determined by:

$$Ev = 0.2S_{\text{DS}} * D$$

S_{DS}: design spectral response acceleration parameter at short periods.

D : effect of dead load

For the horizontal loading, the directional effect of seismic loading was accounted in by considering 100% of the forces for one direction plus 30% of the forces for the perpendicular direction, whichever direction creates the most extreme effect.

Considering the directional and vertical effects of seismic loading the final load combinations for design become:

1. 1.4 D
2. 1.2 D + 1.6 L
3. (1.2 + 0.2S_{DS})D + Ex + 0.3Ey + L
4. (0.9 - 0.2S_{DS})D + Ex + 0.3Ey
5. (1.2 + 0.2S_{DS})D + Ey + 0.3Ex+ L
6. (0.9 - 0.2S_{DS})D + Ey + 0.3Ex

4.1.3 Design of Structural Elements

Figure 4.7: Flowchart for Design of Structural Elements

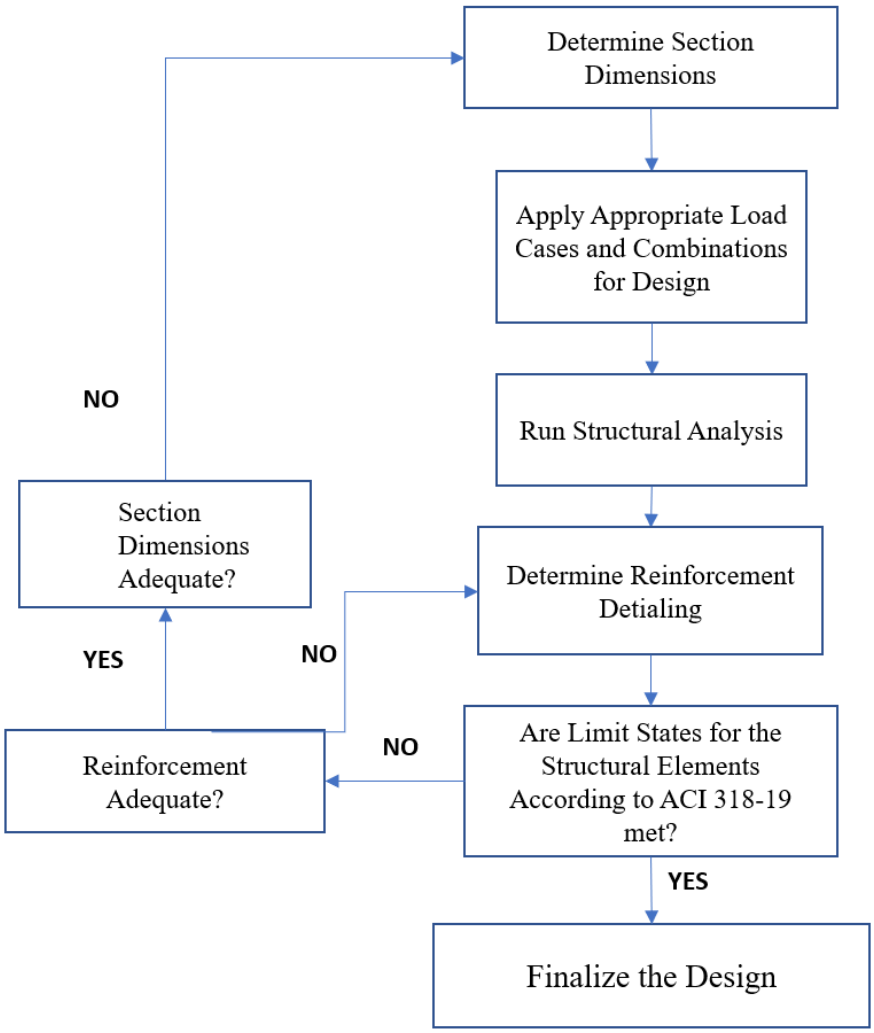

After the design load cases and load combinations were created per ASCE 7- 16 requirements for seismic design, the structural elements were designed.

The sections were assigned appropriate property modifiers specified for the cracked sections in ACI 318-19 Table 6.6.3.1.1 (a). Table 2 Moment of Inertia and Cross-

sectional Areas Permitted for Elastic Analysis at Factored Load Level

Table 4.2: Moment of Inertia and Cross-sectional Areas Permitted for Elastic Analysis at Factored Load Level

Structural Element	Moment of Inertia	Cross-sectional area for axial deformations	Cross-sectional area for shear deformations
Columns	0.70 I_g	1.0 Ag	b_wh
Walls	0.70 I_g	1.0 Ag	b_wh
Beams	0.35 I_g	1.0 Ag	b_wh
Flat Plates and Slabs	0.25 I_g	1.0 Ag	b_wh

4.1.4 Material Properties

Material for the concrete was chosen as C30 and steel material was chosen to be B420C (S420) for the rebars. The material properties can be seen in Table 3.4.

Table 4.3: Material Properties

Material	Modulus of Elasticity (MPa)	Weight per Unit Volume (KN/m^3)	Specified Concrete Compressive Strength f'$_c$ (MPa)	Steel Yield Strength f_y (MPa)
C30	32024.47	23.5642	30.02	-
B420C	200 x 10^3	76.9729	-	420

Two main sources of non-linearity in a structural model are material and geometric non-linearity. The geometric nonlinearity is accounted for in the analysis procedure

by the analysis engine by formulating the equilibrium equations with respect to the deformed geometry at every iteration.
The material non-linearity of reinforced concrete structural elements comes from three main effects:

- Concrete crushing under compression.
- Concrete cracking under tension.
- Steel yielding.

Nonlinearity also arises from the interaction of concrete and steel rebars, such as bond slip, interlocking of aggregate at a crack, and dowel action of the reinforcing bars.[14]
To capture the correct nonlinear behavior of the structural system and understand the mechanical behavior that leads to failure, the appropriate material models are required.
Later, by defining plastic fiber hinges at the appropriate locations, and assigning the correct nonlinear material property to the structural elements, the nonlinearity of the model is ensured.

4.1.4.1 Concrete Material Model

Since at the columns and shear walls the nonlinearity was modeled with nonlinear fiber hinges, the base material assigned to these elements have been modeled with hysteretic properties to ensure nonlineariy. The Takeda hysteresis model was used for the beams and columns and the Pivot hysteresis model was used for the shear walls. For the Pivot model, stiffness degradation and pinching parameters shown in Figure 4.9 were used by taking reference from a study by Dicleli and Durucan [15].

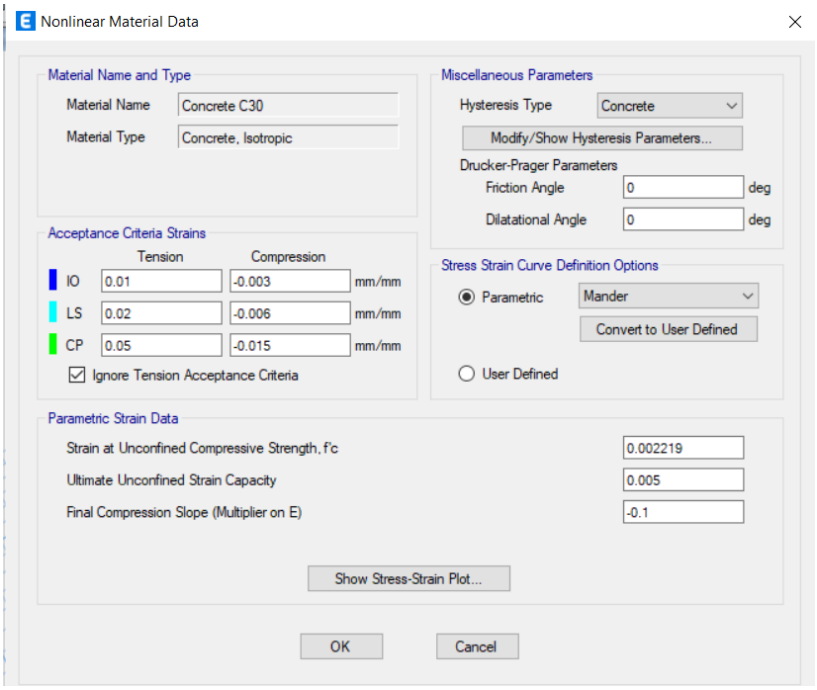

Figure 4.8: Concrete Nonlinear Material Properties in ETABS.

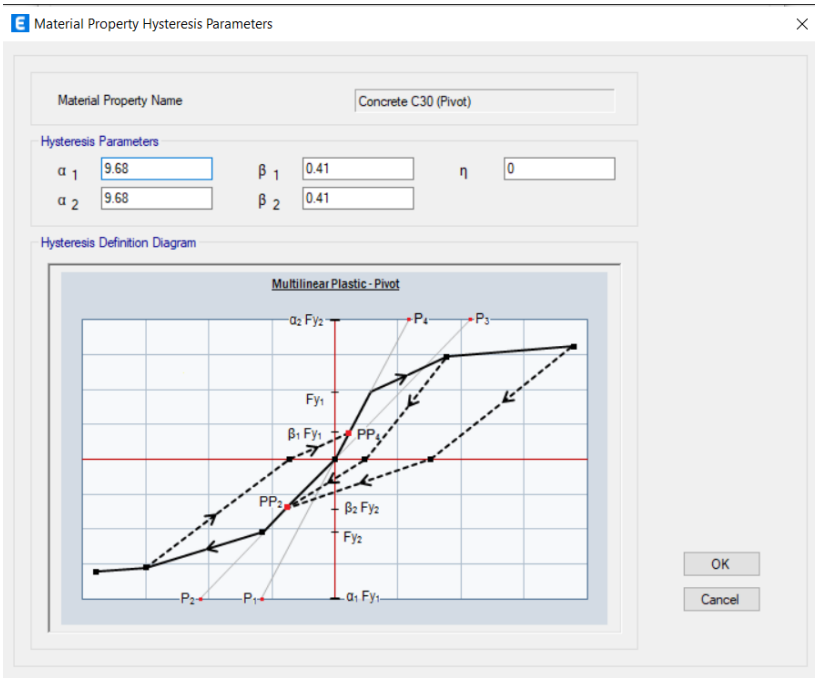

Figure 4.9: Pivot Hysteresis Model

Mander's theoretical stress-strain model for confined and unconfined concrete was

used as the stress-strain model for concrete.

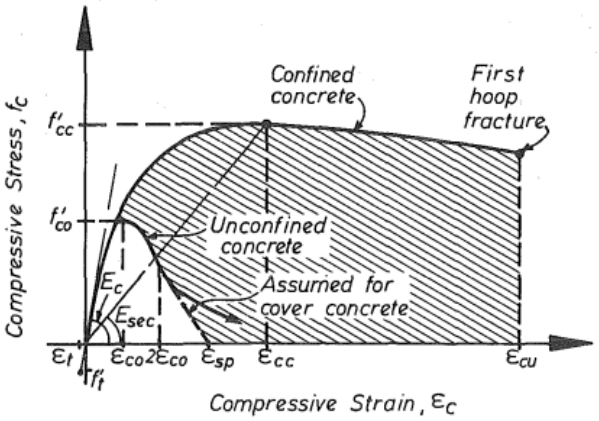

FIG. 1. Stress-Strain Model Proposed for Monotonic Loading of Confined and Unconfined Concrete

Figure 4.10: Mander Material Model [2].

4.1.4.2 Steel Material Models

For steel rebars, the stress-strain material model can be seen in figure 4.11.

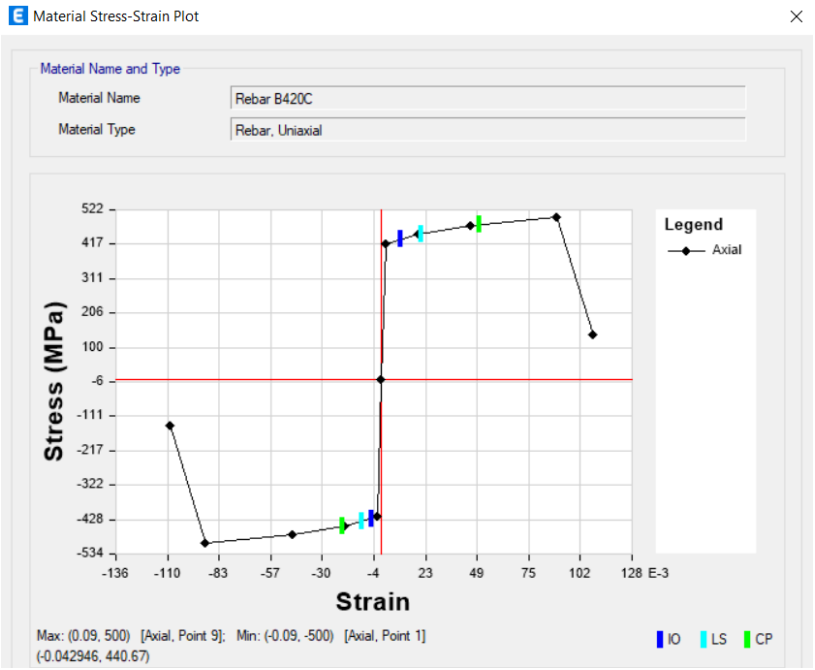

Figure 4.11: Steel Material Model.

4.1.4.3 Column Design

For the design procedure, initial dimensions were determined for the columns, the analysis was conducted under the established design load combinations and the section dimensions were increased as necessary. Clear cover for reinforcement bars is taken as 40 mm. The concrete column sections differ for the first 4 story level and the latter 4 stories. The column section properties can be seen in Table 3. 1

Table 4.4: Column Section Properties

Column Section	Story Level	Width (mm)	Depth (mm)	Clear Cover (mm)	# of Longitudinal Bars	Longitudinal Bar Diameter	Tie Bar Diameter	% Rebar
SD Col 1	1-4	600	600	40	16	#6	#4	%1.26
SD Col 2	4-8	500	500	40	20	#5	#4	%1.34

4.1.4.4 Beam Design

Clear cover for the reinforcement bars is taken as 40 mm. The Beams are 600 mm x 400 mm in dimensions. The detailing of the beams was carried out in ETABS and later for the nonlinear analysis, section properties coming from the design are used in creating the Nonlinear Fibers.

4.1.4.5 Shear Wall Design

On each corner of the building, there are L-shaped shear walls with 300 mm thickness. At the center of the building, there is a 6000 mm x 6000 mm core shear wall which is

500 mm thick. The shear walls are designed as shell elements and labeled as piers to be able to conduct shear wall design in ETABS.

4.1.5 Foundation Design

For this study, isolated square footings were designed under each column and shear wall. There are three different types of footing dimensions for the complete model which are given below:

Table 4.5: Properties of the Foundation

Side Length, B (m)	Thickness, d (m)	Depth of Foundation, D (m)
3	0.5	6
4	0.5	6
8	0.5	6

An Ultimate Bearing Capacity Design was conducted to ensure that the chosen footing dimensions fall in the allowable range of bearing capacity.

The general formula for bearing capacity from Terzaghi's Bearing Capacity Theory (1943) is as follows [16]:

$$q_{\mathrm{u}} = cN_{\mathrm{c}}F_{\mathrm{cs}}F_{\mathrm{cd}}F_{\mathrm{ci}} + \gamma D_{\mathrm{f}}N_{\mathrm{q}}F_{\mathrm{qs}}F_{\mathrm{qd}}F_{\mathrm{qi}} + 0.5\gamma BN_{\gamma}F_{\gamma s}F_{\gamma d}F_{\gamma i} \tag{4.1}$$

The cohesive intercept(c) is zero for sands, c=0. Therefore;

$$q_{\mathrm{u}} = \gamma D_{\mathrm{f}}N_{\mathrm{q}}F_{\mathrm{qs}}F_{\mathrm{qd}}F_{\mathrm{qi}} + 0.5\gamma BN_{\gamma}F_{\gamma s}F_{\gamma d}F_{\gamma i} \tag{4.2}$$

For the square foundations the bearing capacity equation further reduces to;

$$q_{\mathrm{u}} = \gamma D_{\mathrm{f}}N_{\mathrm{q}} + 0.4\gamma BN_{\gamma} \tag{4.3}$$

The N_q and N_γ values are calculated by the following equations:

Friction Angle, ϕ= 35°

$N_q = (1 + sin\phi)$/(1-sinϕ)e$^{\pi tan}\phi$

$N_\gamma = 1.5(N_q - 1)tan\phi$

The calculated bearing capacity parameters for the 3x3 footing are shown on the table below.

Table 4.6: Ultimate Bearing Capacity Parameters

γ	20
D_f	6
B	3
N_q	41.44
N_γ	45.41

The ultimate bearing capacity was calculated as:

$$q_u = 1209.84kN/m^2$$

The factor of safety value (FS) for calculating the allowable ultimate bearing capacity is, FS=3. Therefore, the net allowable bearing pressure is calculated as:

$$q_{\text{u,net}} = q_{\text{u}} - \gamma \, \mathrm{D}_f = 1089.84 kN/m^2$$
$$q_{\text{u,allowable net}} = \frac{q_{\text{u,net}}}{3} = 363.28 kN/m^2$$

The maximum pressure on the footing due to loading is:

$$q_{\text{max}} = 296.33 kN/m^2$$

Which is less than the allowable net pressure, therefore the footing is safe.

4.1.5.1 Modeling of the Soil-Structure Interaction

Table 4.7: Ground Soil Properties

Soil Unit Weight, γ	20 kN/m^3
Poissons Ratio, υ	0.30
Shear Modulus, G	572.680 MPa
Shear wave velocity, Vs	530 kN/m

Gazetas springs are used to account for the soil-structure interaction between the ground and the foundation for each footing.
The surface stiffness equations for the square foundation.

$$\begin{aligned} K_{\text{x,sur}} &= \frac{9 \cdot GB}{2 - \upsilon} \\ K_{\text{y,sur}} &= K_{\text{x,sur}} \\ K_{\text{z,sur}} &= \frac{4.54 \cdot GB}{1 - \upsilon} \\ K_{\text{xx,sur}} &= \frac{3.6 \cdot GB^3}{1 - \upsilon} \\ K_{\text{yy,sur}} &= K_{\text{xx,sur}} \\ K_{\text{zz,sur}} &= 8.3 \cdot GB^3 \end{aligned} \tag{4.4}$$

In order to obtain the embedded stiffness values, the surface stiffness values need to be multiplied by a correction factor.

$$K_{emb} = K_{sur} \times \beta$$

The equations for the correction factor β for each stiffness degree of freedom are given below:

$$\begin{aligned}
\beta x &= (1 + 0.21\sqrt{\frac{D}{B}})[1 + 1.6(\frac{hd(B+L)}{BL^2})^{0.4}] \\
\beta y &= \beta x \\
\beta z &= [1 + \frac{1}{21}\frac{D}{B}(2 + 2.6\frac{B}{L})][1 + 0.32(\frac{d(B+L)}{BL})^{2/3}] \\
\beta xx &= 1 + 2.5\frac{d}{B}[1 + \frac{2d}{B}(\frac{d}{D})^{-0.2}\sqrt{\frac{B}{l}}] \\
\beta yy &= 1 + 1.4(\frac{d}{L})^{0.6}[1.5 + 3.7(\frac{d}{L})^{1.9}(\frac{d}{D})^{-0.6}] \\
\beta zz &= 1 + 2.6(1 + \frac{B}{L})(\frac{d}{B})^{0.9}
\end{aligned} \tag{4.5}$$

d: Height of effective sidewall of the foundation.

h: Depth to the centroid of the footing.

The calculated Gazetas spring stiffness values can be seen on the tables below for a single 3x3 footing are given in tables 4.8, 4.9 and 4.10.

Table 4.8: Calculated Surface Stiffness (K,sur) values

Kx,sur (kN/m)	9095521
Ky,sur (kN/m)	9095521
Kz,sur (kN/m)	11142735
Kxx,sur (kN m/rad)	79520839
Kyy,sur (kN m/rad)	79520839
Kzz,sur (kN m/rad)	14259755

Table 4.9: Calculated Embedment Correction Factors

β_x	1.604
β_y	1.604
β_z	1.407
β_{xx}	1.615
β_{yy}	2.069
β_{zz}	2.037

Table 4.10: Calculated Embedded Stiffness (K,emb) values

Kx,emb (kN/m)	14586278.18
Ky,emb (kN/m)	14586278.18
Kz,emb (kN/m)	15673213.11
Kxx,emb (kN m/rad)	128458946.8
Kyy,emb (kN m/rad)	164539727.4
Kzz,emb (kN m/rad)	29043324.36

4.1.6 Damper Element for Impact Modeling

The aforementioned Impact dampers which were introduced in chapter 3 were used to minimize the structural pounding.

For each rocking column base, the two collapsing bodies to be considered in calculating the impact damping are the column and the isolated footing. The weight of the superstructure is the total amount of dead load applied to the rocking column, and the weight of the substructure is the weight of the footing.

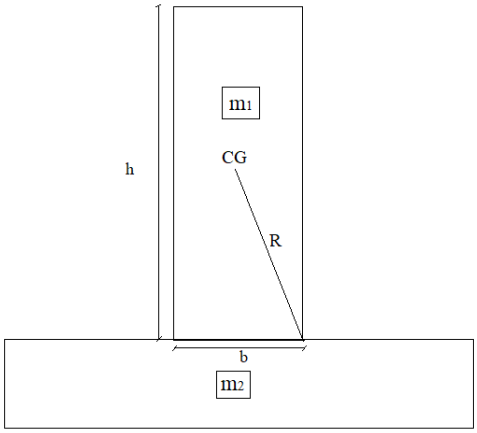

Figure 4.12: Collapsing Bodies

The calculated values for the pounding of the 600 mm x 600 mm column and 3 m x 3 m footing impact damping are shown below.

The weight of the isolated footing, W $_1$ = 106.0389 kN

The weight of the column (with the total weight of the structure applied on the column), W $_2$ = 2123.4442 kN

The axial stiffness of the isolated footing, k $_1$ = 5230.663433 kN/m

The axial stiffness of the column, k $_2$ = 31383.9806 kN/m

The degree of slenderness, α = 11.309 $\circ$

Radial distance to the center of rotation from the center of gravity of the body, R = 1.529 m

Equivalent mass of the two collapsing bodies, M:

$$M = \frac{(m_1 \cdot m_2)}{(m_1 + m_2)} = 100.99kN \tag{4.6}$$

Equivalent stiffness of the two collapsing bodies, k_s:

$$k_s = \frac{(k_1 \cdot k_2)}{(k_1 + k_2)} = 4483.4258kN/m \tag{4.7}$$

The mass moment of inertia $I_o = 4/3MR^2$ = 315.105

Calculation of coefficient of restitution (CR):

$$CR = (\dot{\theta}_2/\dot{\theta}_1)^2 = [1 - \frac{MR^2}{I_\mathrm{o}} \cdot (1 - cos2\alpha)]^2 = 0.009026 \tag{4.8}$$

After obtaining the coefficient of restitution (CR), the damping ratio and the damping coefficient are calculated:

$$\zeta = -\frac{ln(CR)}{\sqrt{(\pi^2 + (ln(CR))^2)}} = 0.83179 \tag{4.9}$$

$$c_\mathrm{imp} = 2 \cdot \zeta \sqrt{k_\mathrm{s} \frac{(m_1 \cdot m_2)}{(m_1 + m_2)}} = 1119.437 kNs/m \tag{4.10}$$

CHAPTER 5

SELECTION OF THE GROUND MOTION RECORDS FROM PEER DATABASE AND NONLINEAR TIME HISTORY ANALYSIS

In this study, the effect of the vertical and horizontal components of ground motion was considered. The test models were subjected to Nonlinear Time History Analysis with direct integration so that the nonlinear elements such as the gap element in ETABS properly work and the nonlinear effects of ground motions can be observed.

5.1 Ground Motion Records

For the Nonlinear Time History Analysis, seven ground motion records were downloaded from the PEER (Pacific Earthquake Engineering Research) ground motion database. The NGA West database was chosen since it is suitable for shallow crustal earthquakes. ASCE Code spectrum option was chosen for the spectrum model.The S_{DS} and S_{D1} values of the target response spectrum were input as the reference point for the search.

After the target response spectrum properties were input, the suitable records were found by searching with the parameters given below:

- Strike Slip + Normal fault types were chosen.
- A 20-50 km range was chosen for the R_{JB} and R_{rup} distances.
- For V_{S30} a range of 360-760 m/s was selected.
- The 8 story building was chosen as reference to scale the ground motion records. The modal period of the building is 0.579. The scaling was done as;

0.2Tn, 0.5Tn, Tn, 1.25Tn, 1.5Tn
Which corresponds to
0.1158, 0.2895, 0.579, 0.7237, 0.8685.

- $D_{5\text{-}95}$ taken 10-60 s.
- SRSS method was chosen for the modal combination and the damping ratio was left as 5%.
- "Minimize MSE" was chosen as the scaling method.

After searching through the database with the given filters, seven ground motions were selected per ASCE 7-16 specifications. At most two ground motion records from the same event were used. The event names, stations, year, magnitude, V_S30, and scale factor values are listed in table 5.1. For the horizontal and vertical directions, two sets of ground motion records were downloaded. Later for analysis purposes, these ground motions were input into the same load case and applied at the same time by applying the same scale factor since these ground motions are simultaneous.

Table 5.1: Selected Ground Motion Records

Event Name	Station	Record Sequence	Year	Magnitude	V_S30 (m/s)	Scale Factor
Landers	Morongo	3756	1992	7.28	368.2	1.2718
Landers	Fun Valley	3753	1992	7.28	388.63	0.9742
Hector	Amboy	1762	1999	7.13	382.93	1.3001
Darfield, New Zealand	Heathcote	6915	2010	7	422	0.5301
Darfield, New Zealand	LPCC	6928	2010	7	649.67	1.0897
Italy	Brienza	288	1980	6.9	561.04	1.3685
Tottori,Japan	SMNH02	3948	2000	6.61	502.66	0.886

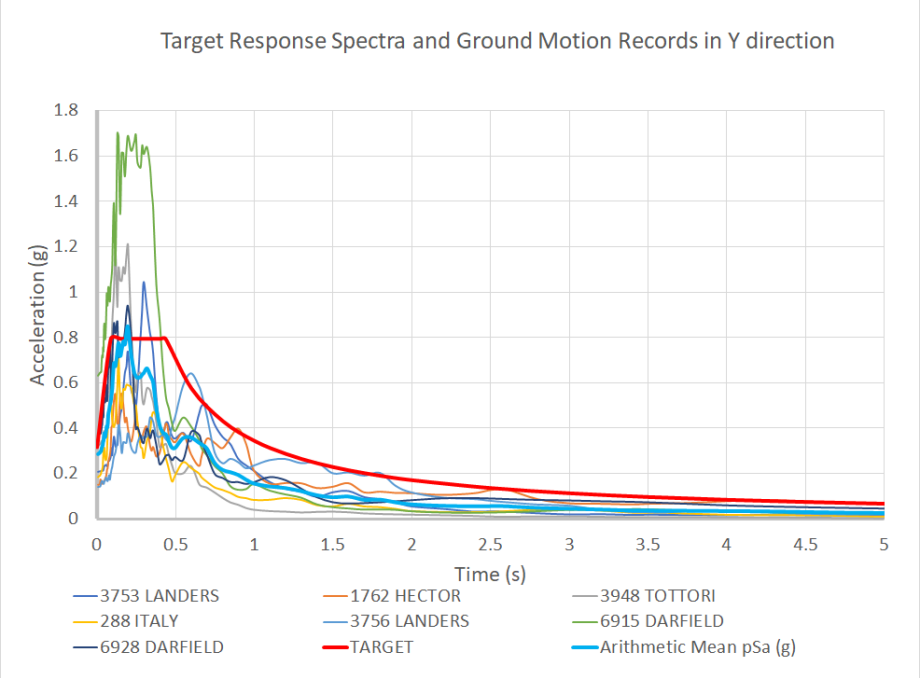

Figure 5.1: Target Response Spectra and Ground Motion Records in Lateral direction

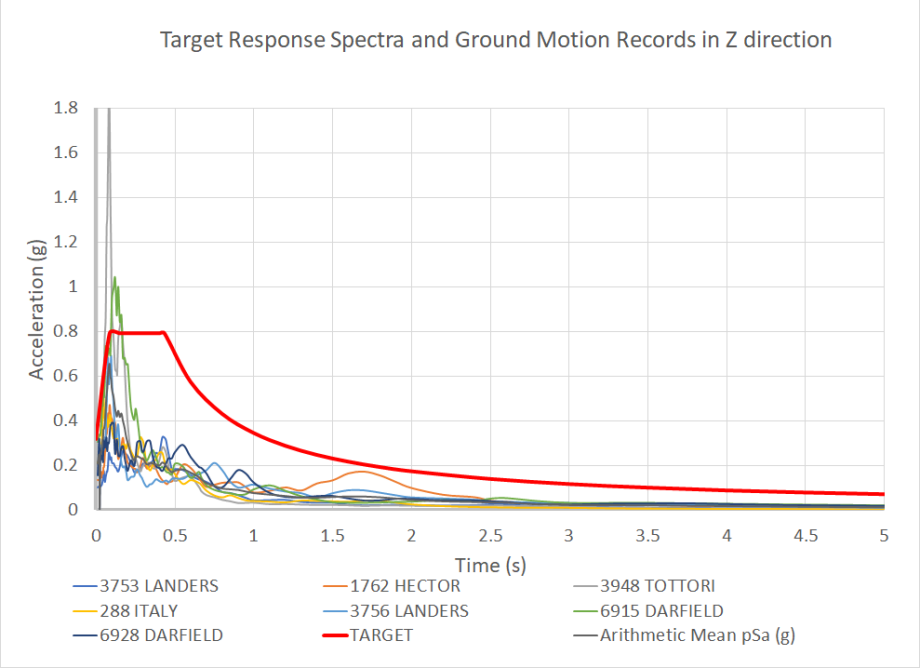

Figure 5.2: Target Response Spectra and Ground Motion Records in Vertical direction

5.2 NTHA Load Case Details in ETABS Software

The aforementioned ground motion records were all applied to the structure in separate NTHA load cases, where the vertical and lateral components of the same ground motion were applied simultaneously. For the analysis, the mass and stiffness proportional coefficients for the models were calculated for NTHA with equations 5.1 and 5.2.

$$\alpha = \frac{4\pi \cdot \xi}{T_1} \tag{5.1}$$

α: mass proportional damping coefficient
T_1: the period of the first mode of the structure
ξ: damping ratio for concrete = 0.02

$$\beta = \frac{w_i \cdot w_j \cdot \xi}{w_i + w_j} \tag{5.2}$$

β: stiffness proportional damping coefficient
w_i: frequency of the first mode
w_j: frequency of the second mode

An example load case definition for Tottori Japan NTH load case preceded by nonlinear static dead load case can be seen in figure 5.3. And the calculated values for mass and stiffness proportional damping can be seen in Figure 5.4.

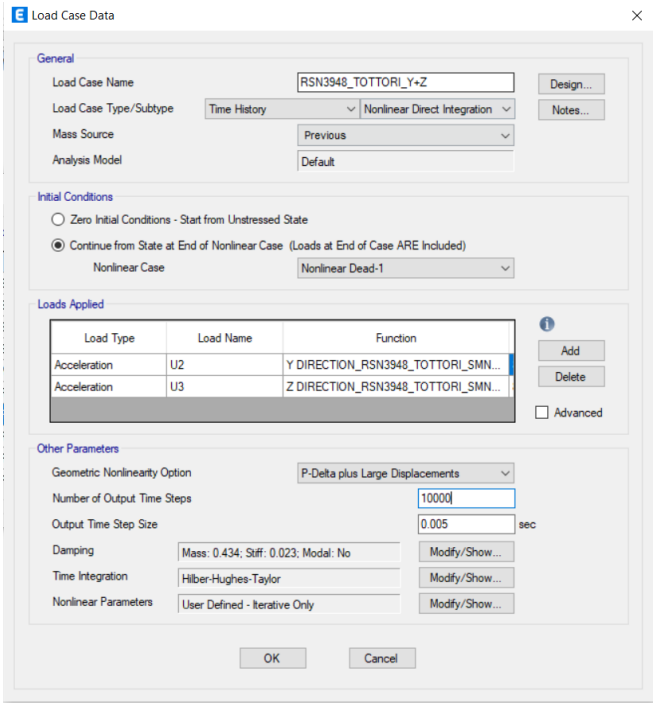

Figure 5.3: NTHA Load Case for 3948 TOTTORI, JAPAN Ground Motion Record

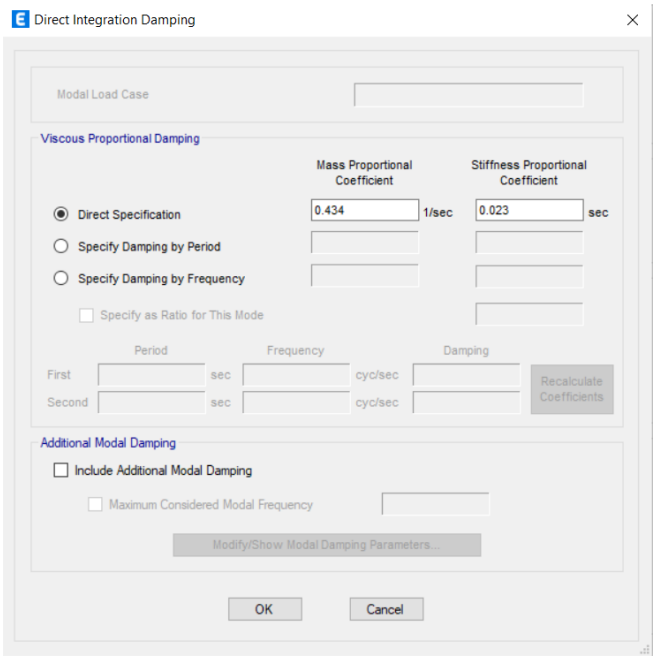

Figure 5.4: Mass and Stiffness Proportional Damping Values Calculated for 8 Story Building Input in ETABS Software

CHAPTER 6

ANALYSIS PROCEDURE AND COMPARISON OF THE ANALYSIS RESULTS

In this study, the rocking-based models were compared with the conventional fixed-based models. In rocking-based models, the uplift is allowed at the outer columns and/or shear walls when the building is viewed from the front, as can be seen in figures 6.1 and 6.2.

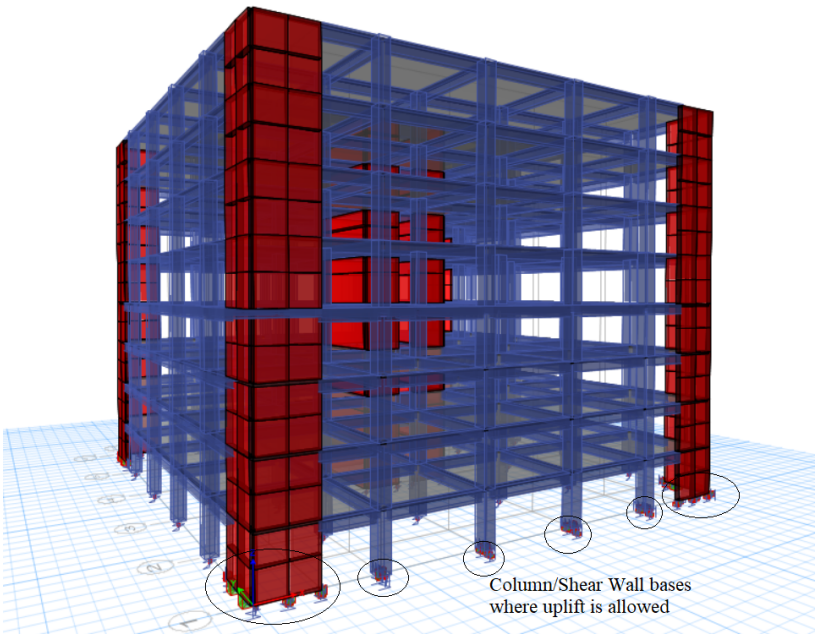

Figure 6.1: 3D View of the Uplift Allowed 8 story Building

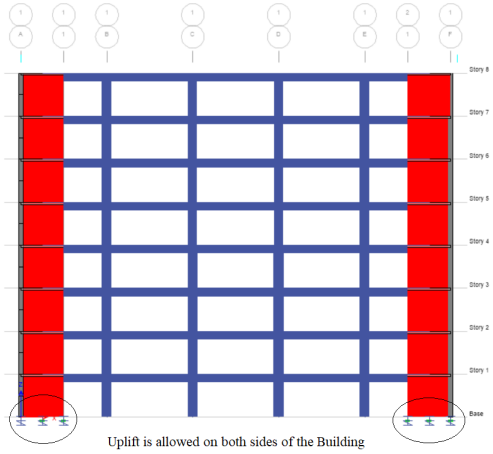

Figure 6.2: Elevation View of the Uplift Allowed 8 story Building

Modeling of the rocking bases is another parameter in this study. Two types of rocking bases were designed, one being a freely rocking based (FRB) columns/shear walls and the other being anchored self centering columns/shear walls with post tensioned strands.

6.1 Modeling of the Rocking Base

For the comparative study, different parameters were accounted for in the modeling procedure of the rocking-based energy dissipation system. The alternatives for the rocking base system are:

- Free Rocking Base (FRB): Rocking columns free to rock with no restraints at the base.
- Rocking Base Equipped with Post-Tensioned Strand (PT Rocking Base): Rocking columns equipped with re-centering post-tensioned strands at the base.

6.1.1 Free Rocking Base (FRB)

Despite being popular in research the rocking-based columns are not readily implemented in conventional building design and analysis software, therefore, an additional

effort is required by combining different types of elements to obtain the finite element modeling of the rocking-based columns. For the case where the columns/shear walls are able to rock at the base a different use was made out of "Gap" elements in ETABS software. The gap elements acting in the vertical direction allow the uplift of the column but have stiffness in the compression direction which mimics the column standing on the footing. To be able to mimic this behavior the gap elements act in the +Z direction and have a 0 mm gap length. The gap elements acting in the Y axis allow a certain amount of lateral displacement which was optimized as 100 mm for the columns, therefore the gap length is 100 mm in each direction for these elements. This is the idealization of a rocking column sitting on a steel shoe in real-life application.

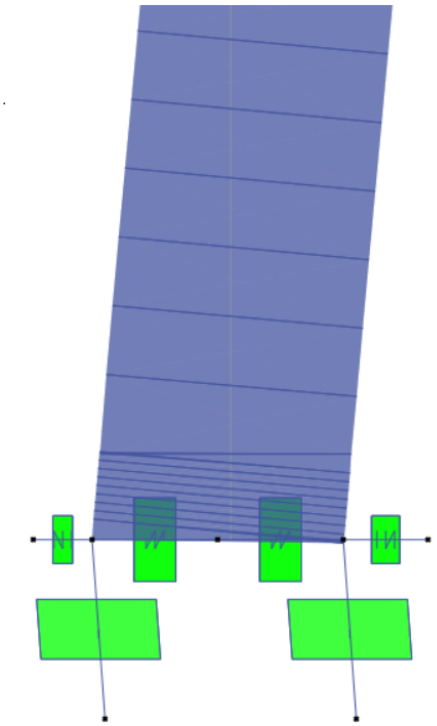

Figure 6.3: Free Rocking Column Base

6.1.2 Rocking Column Equipped with Post-Tensioned Strand (PT Rocking Columns)

For the case with the self-centering columns equipped with post-tensioned unbonded tendons, the tendon going through the rocking columns is modeled as load in ETABS

software. At the base where the strand is anchored to the footing, the strand is modeled with a link at the base with appropriate section and material property to the link element in ETABS software.

The uplift-allowed model was modeled with nonlinear gap springs which have rigid stiffness under compression and no stiffness under tension. This allows the outer edges of the building to uplift under seismic loads. In addition, as part of the parametric study, later, linear dampers were added to the system to the uplift-allowed columns and shear walls to soften the behavior under dynamic loads.

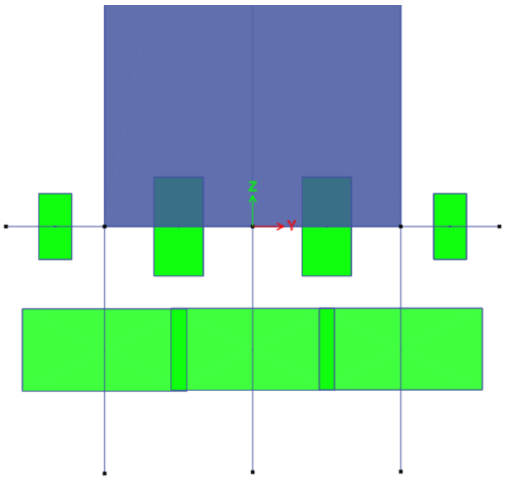

Figure 6.4: Rocking Base with PT strand

6.2 Analysis Models

For simplicity, the analyses were conducted in 2D plane rather than 3D. The models were simplified by taking a strip in the YZ plane and narrowing down the active degrees of freedom to the two-dimensional YZ plane; Uy, Uz, and Rx. This way, it is ensured that the analysis time is optimal and the effects of the uplift can be observed in a narrower scope. The strips that are taken from the models are the A-A and B-B planes shown in the figure below to be able to account for the cases with RC frame only as well as the Shear Wall-RC system.

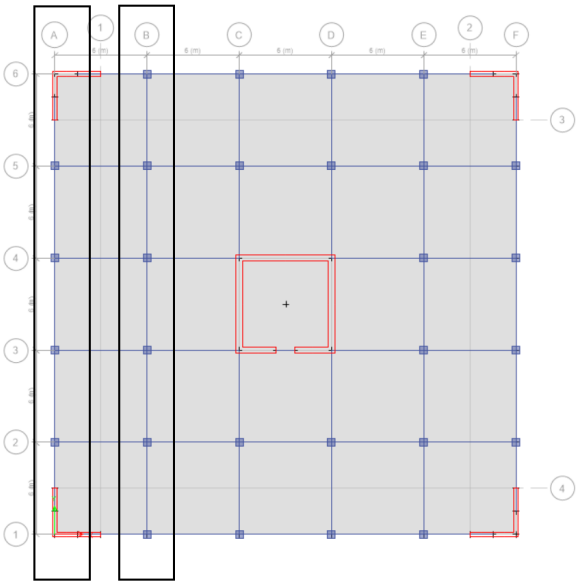

Figure 6.5: Plan View of the Building highlighting BB and AA planes

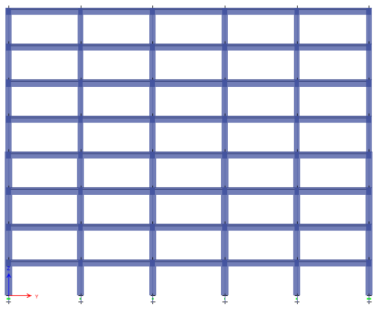

Figure 6.6: Elevation View of the BB plane of 8 story building

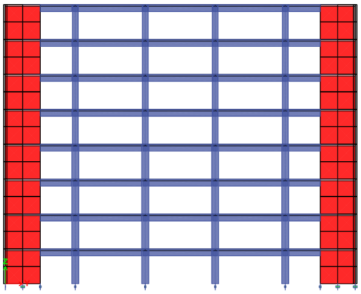

Figure 6.7: Elevation View of the AA plane of 8 story building

The test models for this study consist of variations of the AA-Plane (with shear walls) and the BB-Plane (without shear walls) models. The complete set of the analysis models is given in Figure 6.8.

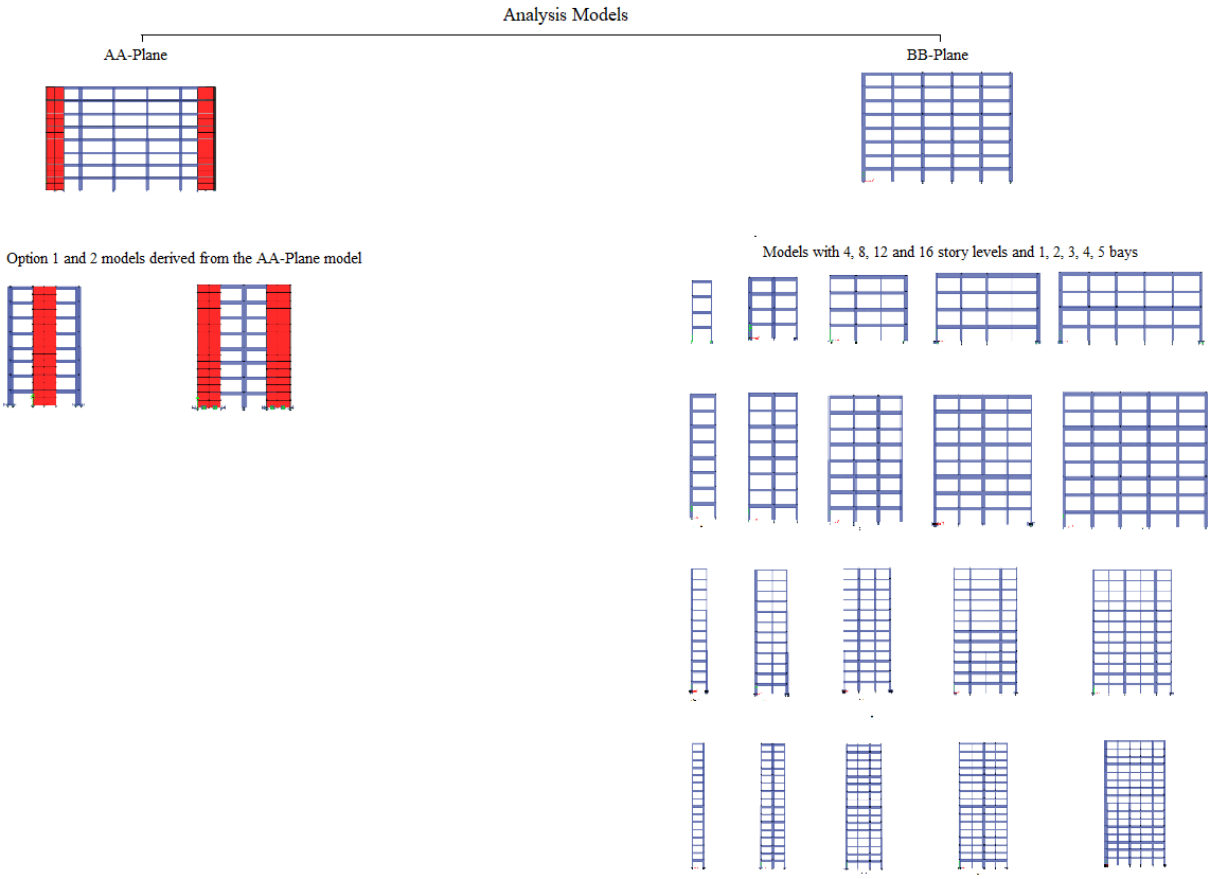

Figure 6.8: Analysis Models

6.3 Free Rocking Base (FRB) Analysis and Comparisons

Firstly, the aforementioned two frames were compared under NTHA cases.

6.3.1 Comparison of the Model with Shear Walls (AA-Plane) and Model without Shear Walls (BB-Plane)

For the model with shear walls and the model without shear walls, first, the free rocking base (FRB) models were compared with the fixed based models of the benchmark model, 8 story 5 bay frame. The analysis was conducted under Landers 3756 NTH load case, which was chosen since it provided the closest results to the average of a total of seven ground motions.
For the model without shear walls, the rocking base case showed significant improvement in results(up to 10 % reduction in base shear) which will later be elaborated. For the shear walled frame case, the analysis results show that uplift under NTHA is not as effective as in the model without shear walls and the difference between the rocking and fixed base cases is much smaller (about 0.01 % difference in story shear force results at best in AA-Plane model) as can be seen in plots on Figure 6.10.

To investigate these two cases further, the same ground motion was scaled to have different intensities, 0.25 g, 0.5 g, 0.75 g, and 1 g. The base shear and base moment ratios of the FRB cases to the fixed base cases were observed to reduce with increasing intensity for both cases(Figure 6.9). Implying that the rocking is more effective as the ground motion intensity increases.

	AA-Plane Model		BB-Plane Model	
NTH Load Case	**Base Shear Force Ratios (FRB /Fixed)**	**Base Moment Ratios (FRB /Fixed)**	**Base Shear Force Ratios (FRB /Fixed)**	**Base Moment Ratios (FRB /Fixed)**
0.25 g	1.0229	0.9993	0.9321	1.0113
0.5 g	1.0145	1.0011	0.9026	0.9092
0.75 g	0.9840	0.9964	0.8948	1.0164
1 g	0.9819	1.0009	0.8366	1.0027

Figure 6.9: The Base Shear and Base Moment Ratios of Free Rocking Based (FRB) models to Fixed Base Models under different ground motion intensity levels

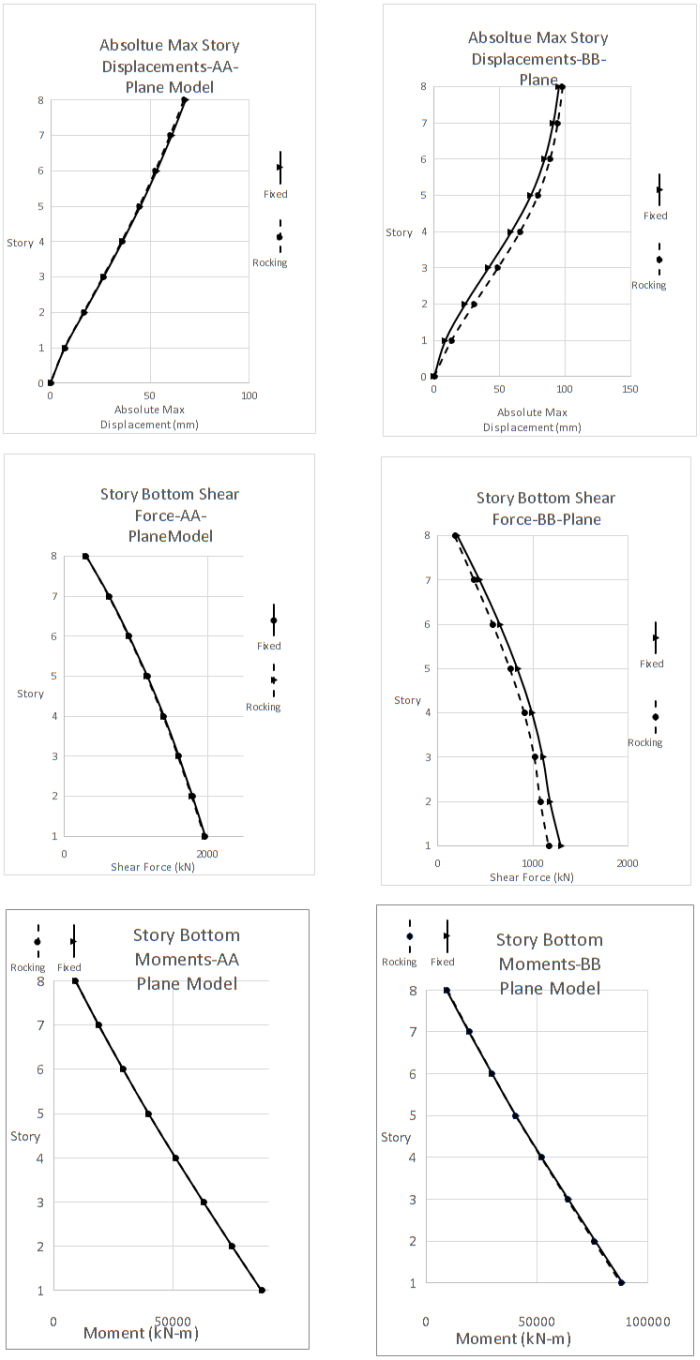

Figure 6.10: Absolute Max. Displacement, Story Shear Force, and Story Moment Results of Frame with Shear Walls (AA-Plane) and Frame without Shear Walls (BB-Plane) Models for 0.5 g

6.3.2 Comparison of the Shear Walled Frame (AA-Plane) and Option 1 and Option 2 Models

To be able to test and account for the different number of bays on the shear walled model, two other models were created in addition to the AA-Plane frame of the building, Option 1 and Option 2 which are variations of the shear walled model with fewer number of bays and different configurations. The story bottom shear force and absolute maximum displacement results were compared for these models also, these can be seen in Figure 6.11.

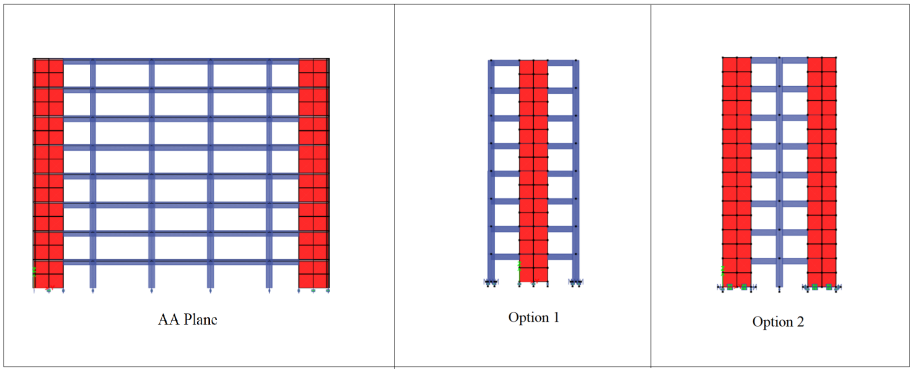

Figure 6.11: Elevation view of the AA-Plane, Option 1 and Option 2 models

As can be seen in the plotted results on Figure 6.12, the rocking based and fixed models do not show a prominent difference in shear walled frame models AA-Plane, Option 1 and Option 2.

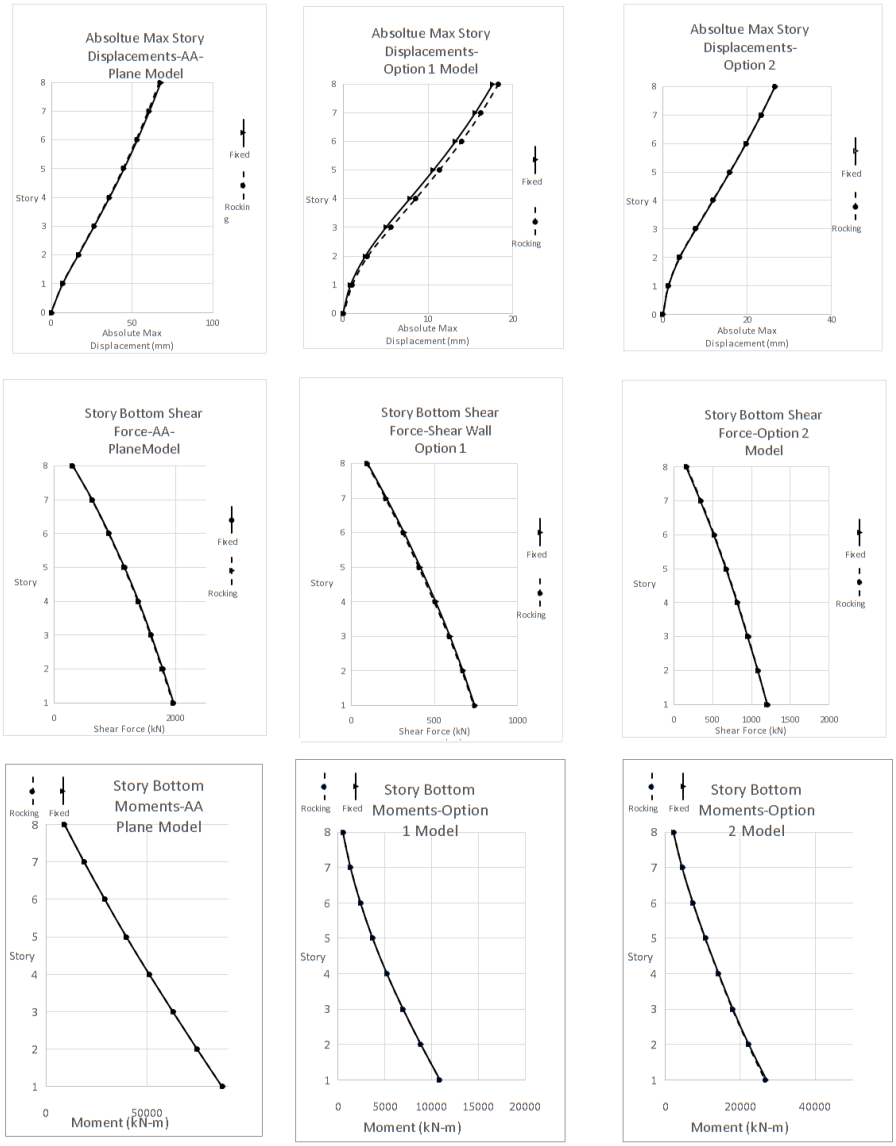

Figure 6.12: Absolute Max. Displacement and Story Shear Force Results of the AA-Plane, Option 1 and Option 2 models

From the story shear and displacement results, it can be seen that in the Option 1 model there is some amount of uplift. This uplift occurs at reinforced concrete outer columns. Whereas for the other models, AA-Plane and Option 2, there is no visible difference. From the comparison of these three models, it can be observed that the rocking outer shear walls do not show significant improvement compared to the conventional fixed base case results. The size and shape of these shear walls are presumed to be the reason.

6.3.3 Comparisons for the Model without Shear Walls (BB-Plane Model)

To continue with the study with further comparisons, the BB Plane model was used in analyses since it was concluded that the shear-walled frames do not perform as well as the models without shear walls.

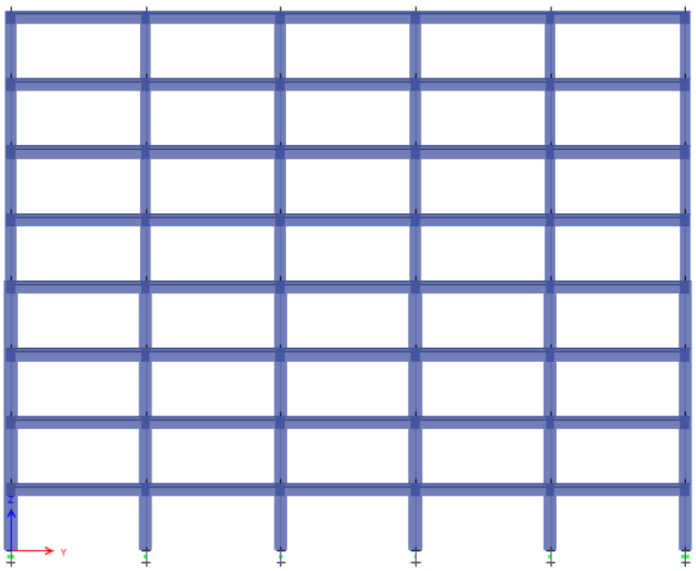

Figure 6.13: Model without Shear Walls (BB-Plane)

6.3.3.1 Analysed Under Different Ground Motion Intensity Levels

The 8-story 5-bay model with FRB was compared to the conventional fixed base case. In the previous comparison between the models with and without shear walls, it can be seen in Figure 6.9 that as the intensity of the ground motion increases, the rocking isolation is more effective. In Figure 6.15, the Base Shear-Time graphs were plotted for the model without shear walls for the fixed and FRB cases. In these plots, it can be seen that the differences between the spikes of FRB and fixed cases slightly increase as the intensity increases. The same comparison was carried out for the 8-story 1-bay model as well (Figure 6.15) which is the extreme case of the benchmark model. The differences are higher for the extreme case due to the difference in number of bays which will be further elaborated in Chapter 6.3.6.

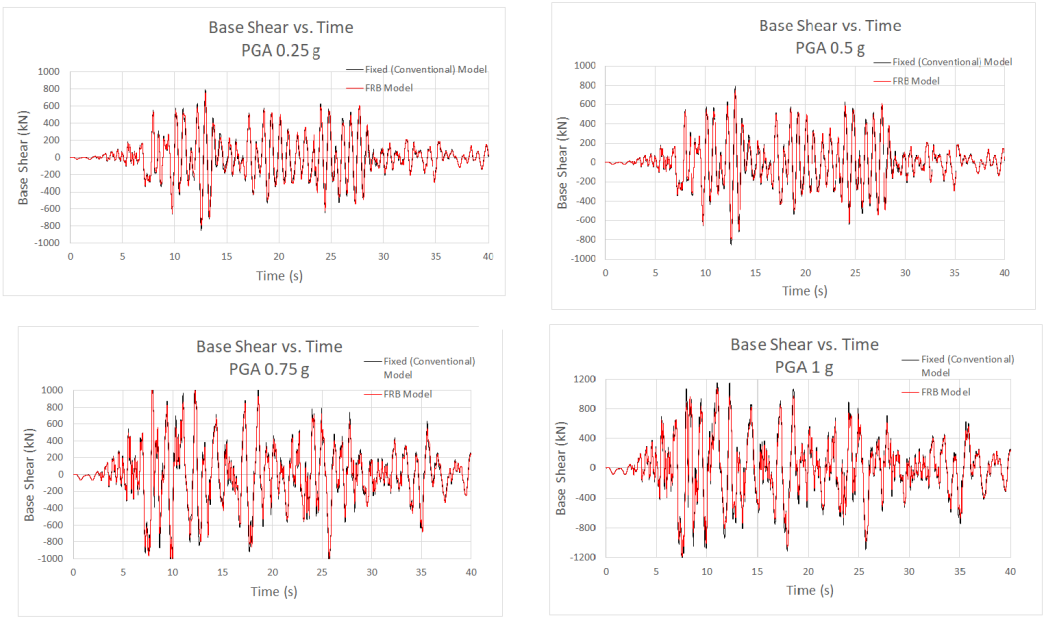

Figure 6.14: FRB and Fixed base shear forces plotted with respect to time for different ground motion intensity levels for the 8 story 5 bay case

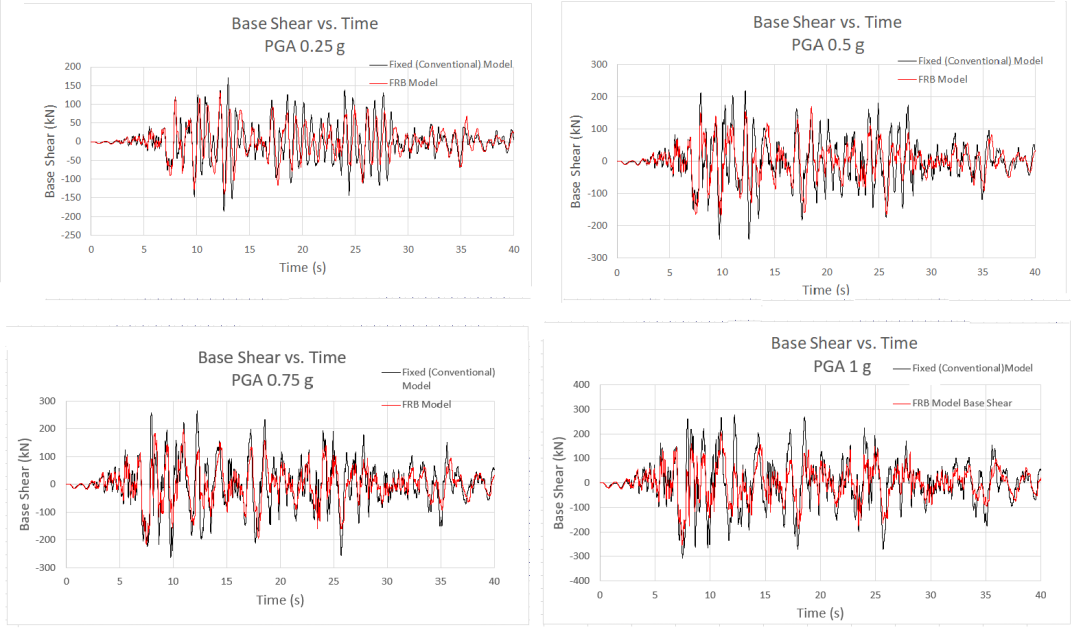

Figure 6.15: FRB and Fixed base shear forces plotted with respect to time for different ground motion intensity levels for the 8 story 1 bay case

6.3.3.2 Hysteresis Loops of the Model without Shear Walls

In addition to the comparisons under different ground motion intensity levels, base shear versus roof displacement values were plotted to see the difference in the hysteretic behavior of the fixed base and FRB cases for both 8 benchmark case of 8-story 5- bay and extreme case 8-story 1-bay case. In Figures 6.16 and 6.17, the separate and joint plots of the fixed base and FRB cases can be seen. On the joint plots, it can be observed that the FRB case has better performance under seismic loading.

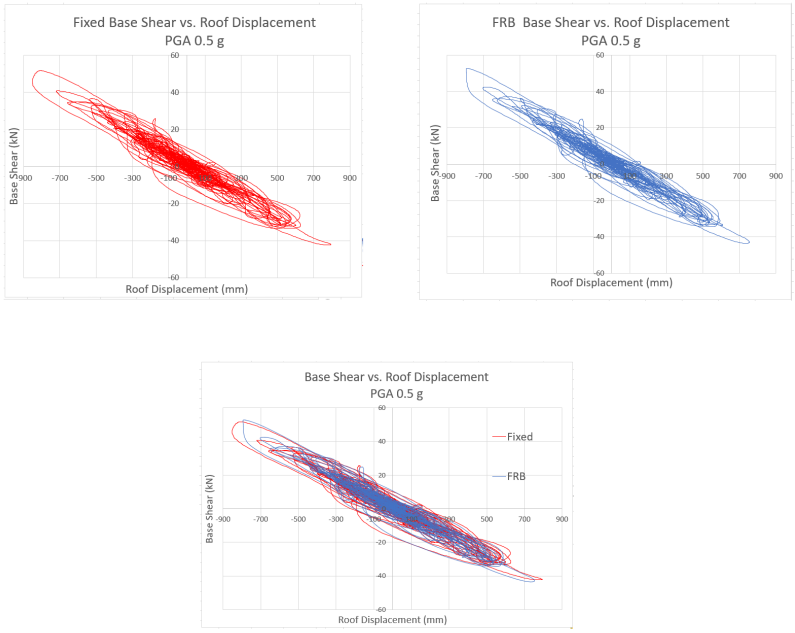

Figure 6.16: FRB and Fixed base shear force versus roof displacements for the 8 story 5 bay case

Figure 6.17: FRB and Fixed base shear force versus roof displacements for the 8 story 1 bay case

6.3.3.3 Hinge Rotations of the Model without Shear Walls

The hinge rotations of the FRB case and the fixed base case were compared to see the effect of the free rocking base at the element level.
The fixed and FRB models were subjected to a nonlinear time history load case with the ground motion intensity level of 1 g for this comparison.

The hinges at story 1, story 4, and story 6 beams were compared in terms of rotation. As per the code requirements, the behavior is adjusted in the design so that the initial plastic hinging occurs at beams rather than columns. The hinging of the fixed based model can be seen in figure 6.18.

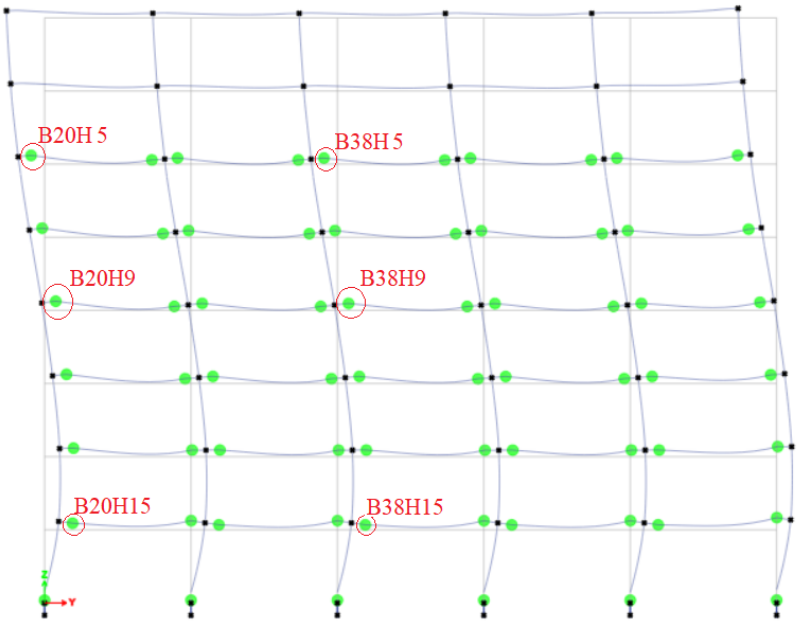

Figure 6.18: Fixed base model hinging under 1 g intensity ground motion

The comparison of corresponding hinge rotation over yield rotation values for the fixed based and FRB models can be seen in figure 6.19.

		Fixed Based	FRB
Story	Hinge	$\theta_{plastic}/\theta_{yield}$	$\theta_{plastic}/\theta_{yield}$
1	B38H15	5.6618	7.0588
4	B38H9	5.4412	1.4559
6	B38H5	5.0147	4.0074
1	B20H15	5.0662	11.7353
4	B20H9	6.3750	1.5515
6	B38H5	6.4485	1.1985

Figure 6.19: Plastic rotation over yield rotation values

It can be seen from the tabulated results that at the element level the hinge rotations are generally less in the FRB case compared to the fixed base case except for the slight differences at the hinges on the story 1 level. Later, viscous linear dampers are added to the system at the story 1 level to soften the behavior at the first story level as well.

6.3.3.4 Different Numbers of Stories and Bays

As mentioned briefly in Chapter 4, four different story-level buildings were designed for this study; 4, 8, 12, and 16 stories. Another parameter in this study is the number of bays. 2D frames without shear walls were analyzed for every story level and for the number of bays; 1,2, 3, 4, and 5. The analyses were conducted for seven different ground motion records downloaded from the PEER ground motion database.

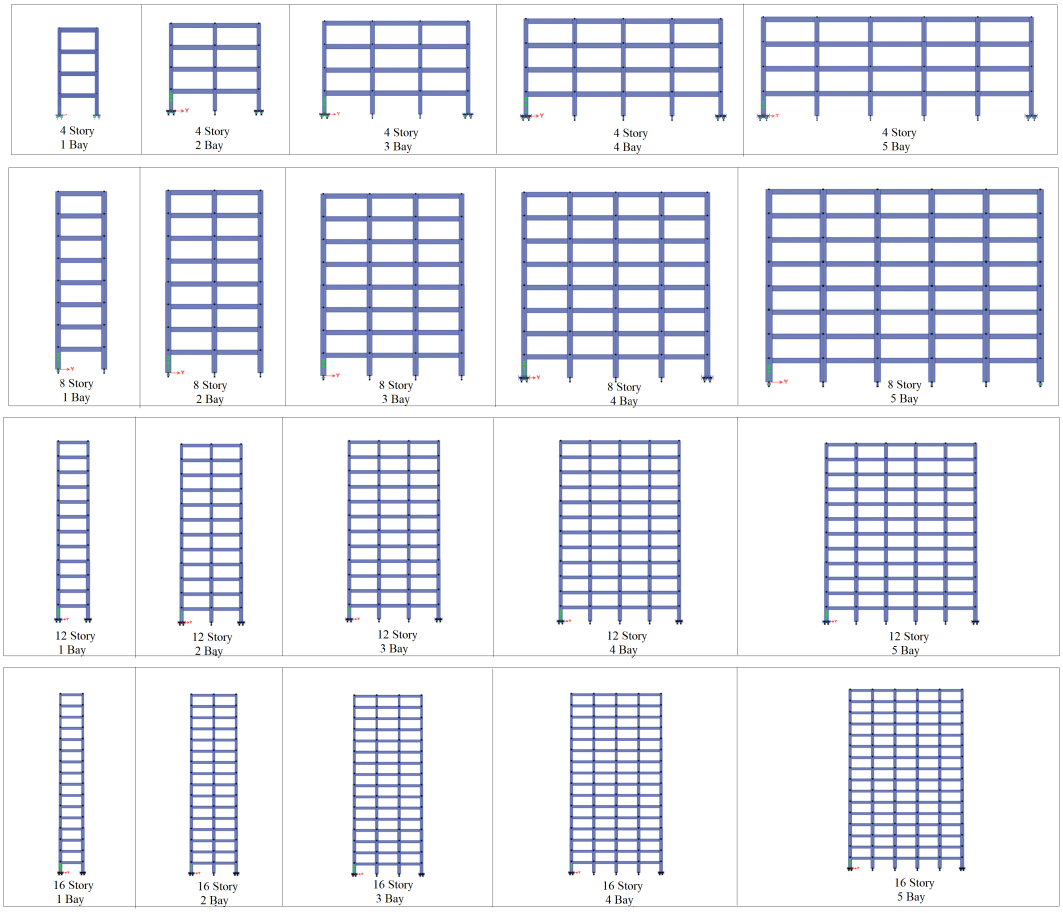

Figure 6.20: RC Frames with Different Stories and Bays

The average of the seven NTHA results was compared for total base shear and total base moment ratios. The comparison of results for the different story levels and the number of bays can be seen in Figures 6.21, 6.22, and 6.23.

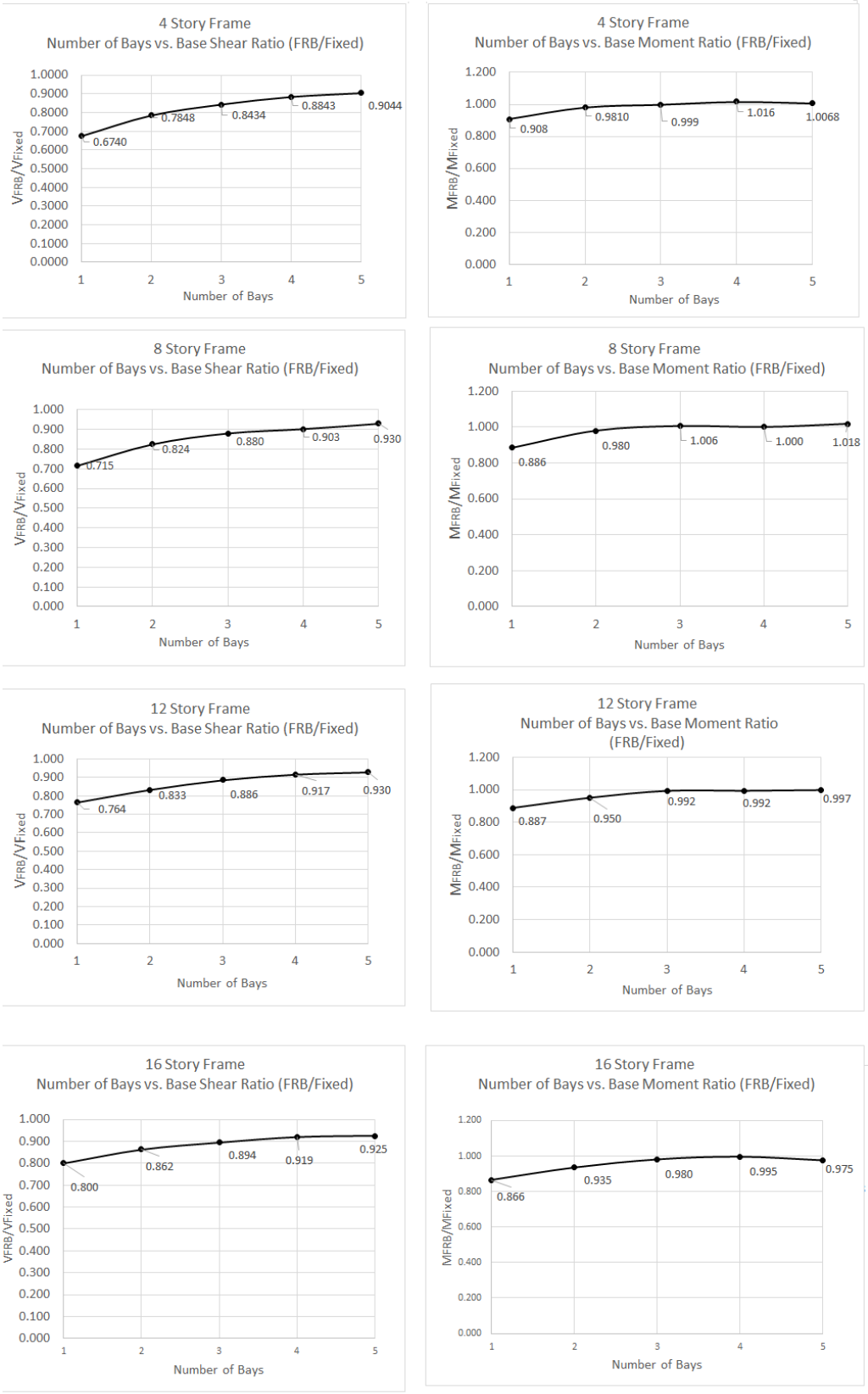

Figure 6.21: The Base Shear and Base Moment Ratios of Free Rocking Based (FRB) models to Fixed Base Models Plotted for 4,8,12 and 16 Stories in Varying Number of Bays

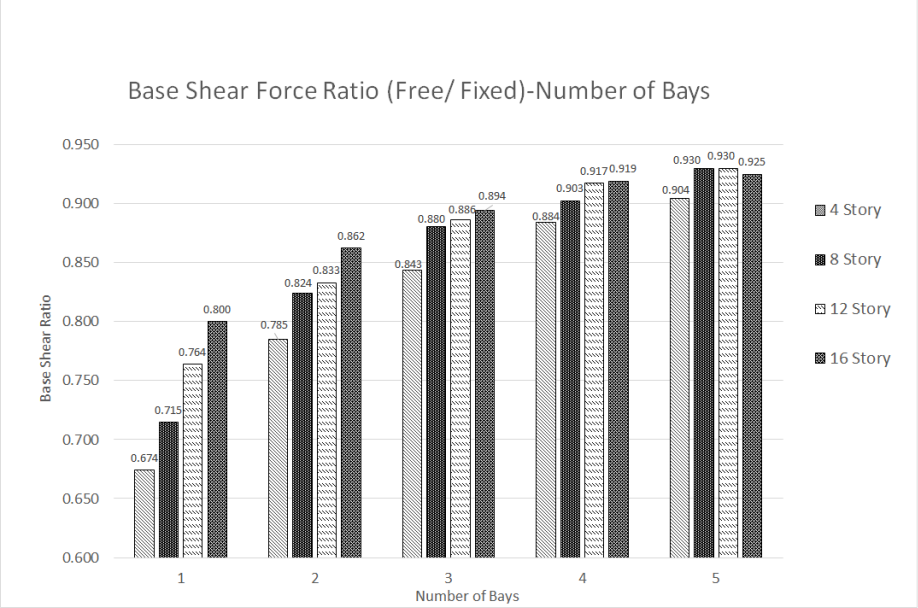

Figure 6.22: The Base Shear Ratios of Free Rocking Based (FRB) models to Fixed Base Models Plotted for 4,8,12 and 16 Stories in Varying Number of Bays

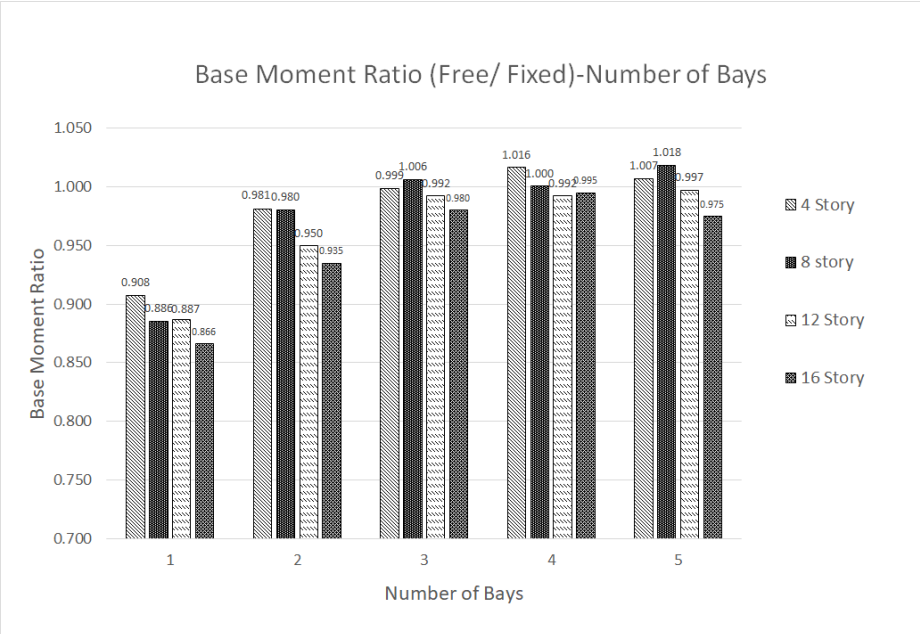

Figure 6.23: Base Moment Ratios of Free Rocking Based (FRB) models to Fixed Base Models Plotted for 4,8,12 and 16 Stories in Varying Number of Bays

As can be seen in plots 6.21 and 6.22 and 6.23, as the number of stories increases,

the base shear force ratio of the rocking (free) case to fixed case increases. And as the number of bays increase along the same story level, this ratio again, increases. Therefore, it can be observed that the effect of rocking outer columns on the seismic performance of the structure increases at lower story levels, performing best at the 4-story level and worst at the 16-story level. In addition, as the number of bays increases, the effect of rocking outer columns decreases. This is the expected behavior since the slenderness ratio of the building decreases as the number of bays increases.

Similarly, for the base moment case as the number of bays increases, the seismic performance of the frames is reduced. But contrary to the base shear force case, as the story height increases, the free (rocking)/fixed moment ratio decreases, which suggests with the increasing story levels the base moment is further reduced for the free (rocking) outer column case. This is also expected since as the number of stories increases, the frames become more flexible under in-plane bending.
To observe the effect of the different numbers of bays solely, another test was conducted by only focusing on the benchmark problem of the 8 story frame. The story drift and shear force results under the 3756 Landers load case can be seen in Figures 6.24, 6.25, 6.26, 6.27, and 6.28. The 3756 Landers load case was chosen for comparison since it is the load case that provides the closest results to the average of seven ground motion records.

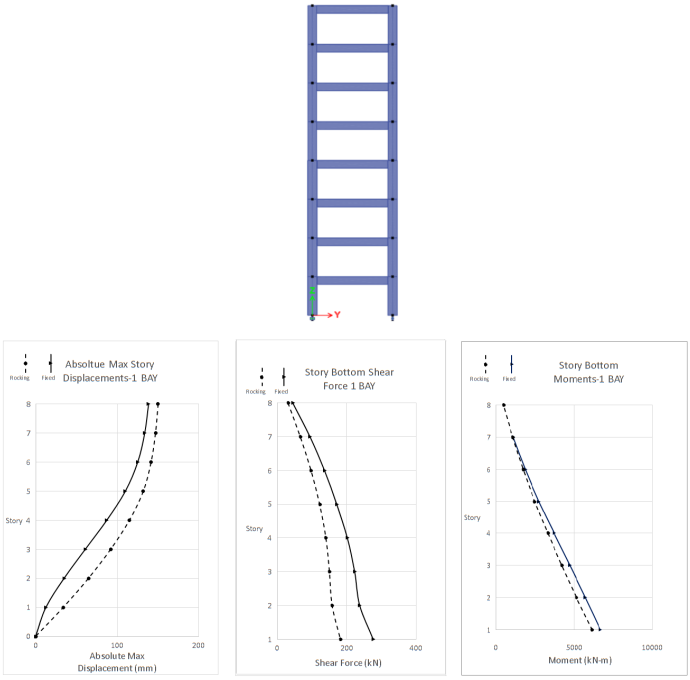

Figure 6.24: Story Displacement and Shear Force Results for 8 Story 1 Bay Frame

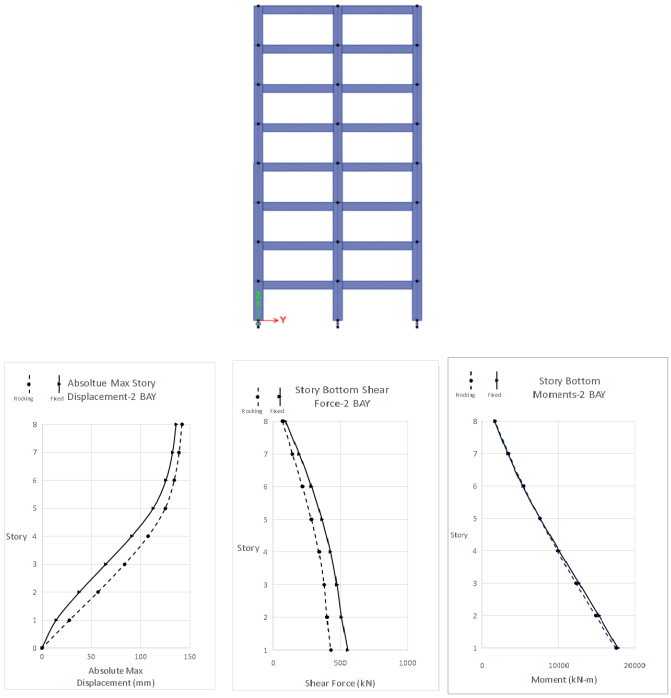

Figure 6.25: Story Displacement and Shear Force Results for 8 Story 2 Bay Frame

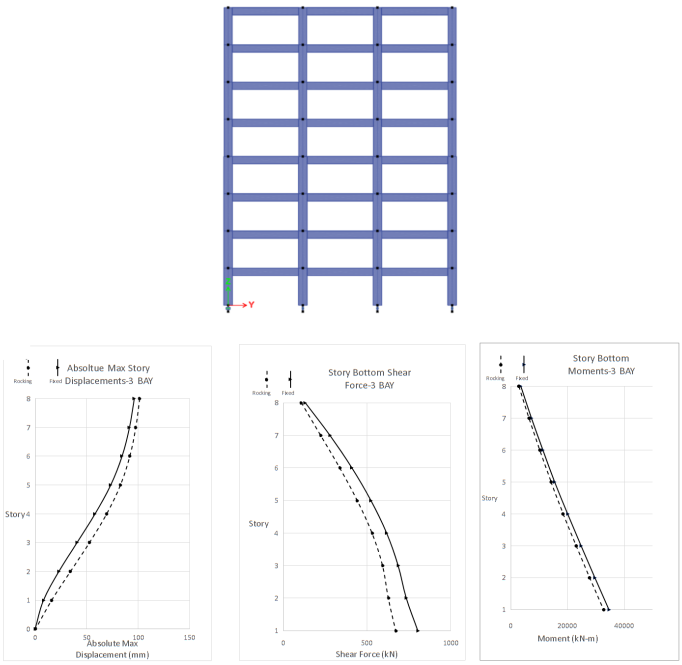

Figure 6.26: Story Displacement and Shear Force Results for 8 Story 3 Bay Frame

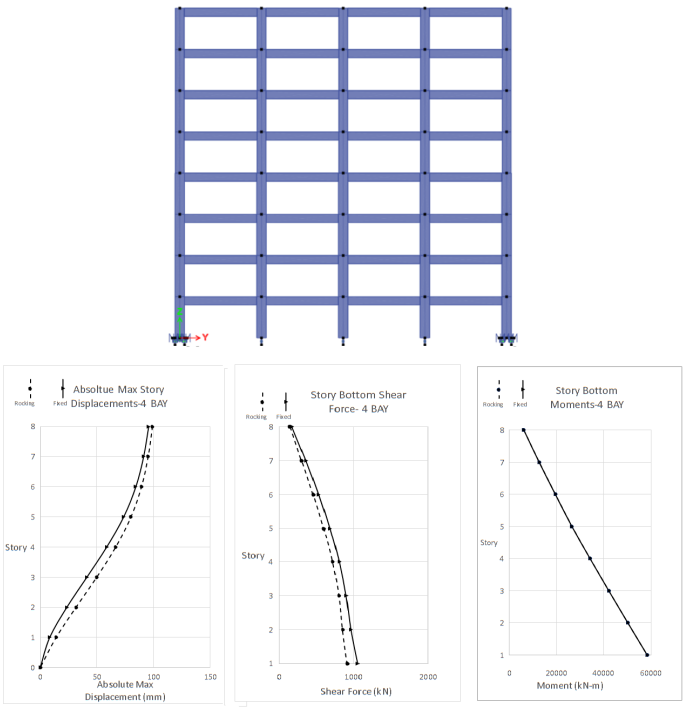

Figure 6.27: Story Displacement and Shear Force Results for 8 Story 4 Bay Frame

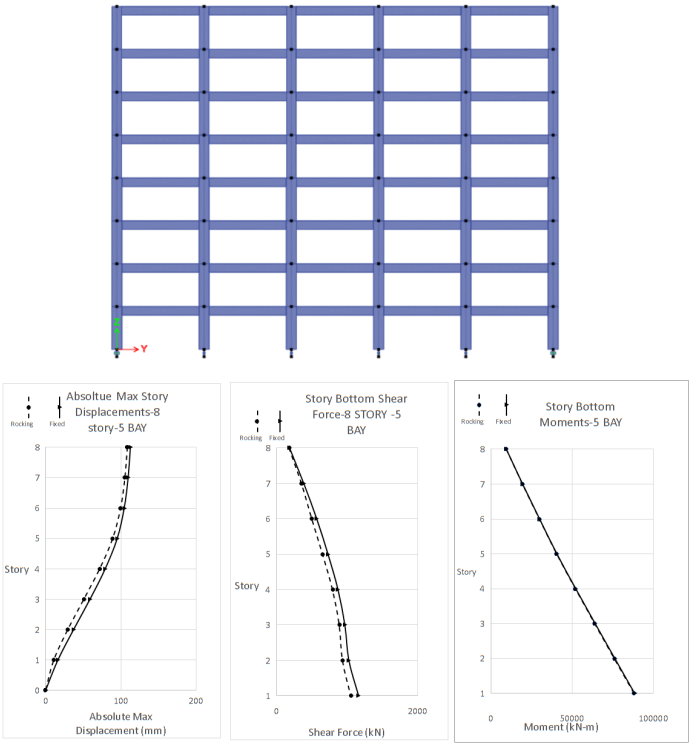

Figure 6.28: Story Displacement and Shear Force Results for 8 Story 5 Bay Frame

The base shear and moment ratios of these models are also given in Figure 6.29.

	Base Shear Force Ratio (Rocking/Fixed)	Base Moment Ratio (Rocking/Fixed)
8 Story, 1 Bay	0.6386	0.8711
8 Story, 2 Bay	0.8092	0.9078
8 Story, 3 Bay	0.8292	0.9626
8 Story, 4 Bay	0.8613	0.9724
8 Story, 5 Bay	0.9000	0.9941

Figure 6.29: Base Shear Force and Base Moment Ratios for the 8 story model for different number of bays

It can be seen from these results that the effect of rocking columns to general response is high even for the least effective 5 bay case where the total reduction on base shear is up to 10 %.

6.4 Comparison of Fixed and Free Rocking Base (FRB) Models Improved with Dampers

In order to improve the effect of rocking on the performance of the frame, vertical fluid viscous dampers were added to story 1 at the base of the uplifting columns as illustrated in figure 6.30.

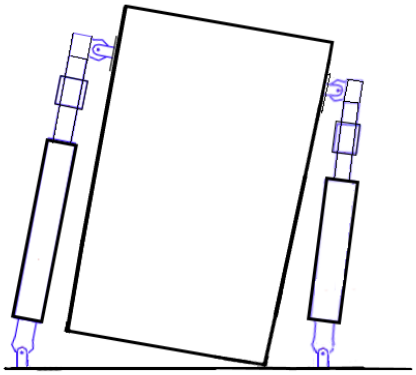

Figure 6.30: Vertical fluid viscous dampers at free rocking base

The equation for exponential damping force is given, Eqn. 6.1.

$$F_{\mathrm{d}} = c \cdot V^{\alpha} \tag{6.1}$$

F_d: damping force

c: damping coefficient

V: particle velocity

α: damping exponent

For the parametric study, the damping exponent, α, and the damping ratio, c, values were controlled. F or the damping coefficient value, different multiples of the maximum uplift force under time history analysis case **Landers 3756**, F_u=1214 kN was taken.

For testing the effect of the α parameter, the c value was taken constant to be c=0.5F_u. The set of models for this case is specified in Table 6.1.

Table 6.1: Different Parameters for α where the c value is controlled

Model	α	c
Model 1	0.005	0.5F_u
Model 2	0.5	0.5F_u
Model 3	1	0.5F_u
Model 4	1.5	0.5F_u
Model 5	2	0.5F_u

In order to see the effect of the c value, the α parameter was controlled and taken constant at α=1. The set of models for this case is specified in Table 6.2.

Table 6.2: Different Parameters for c where the α value is controlled

Model	α	c
Model 1	1	0.25F_u
Model 2	1	0.5F_u
Model 3	1	0.75F_u
Model 4	1	F_u

In order to save computational time and overcome the convergence issues, the analyses were conducted in 8 story 1 bay model. The plastic hinge results were compared for these models by taking the hinging of first-story beam B20 into account.

For comparison, the ratios of the plastic hinge rotation at the end of 3 times **Landers 3756** load case (making intensity 1.5 g) to yield hinge rotations were obtained for all the models.

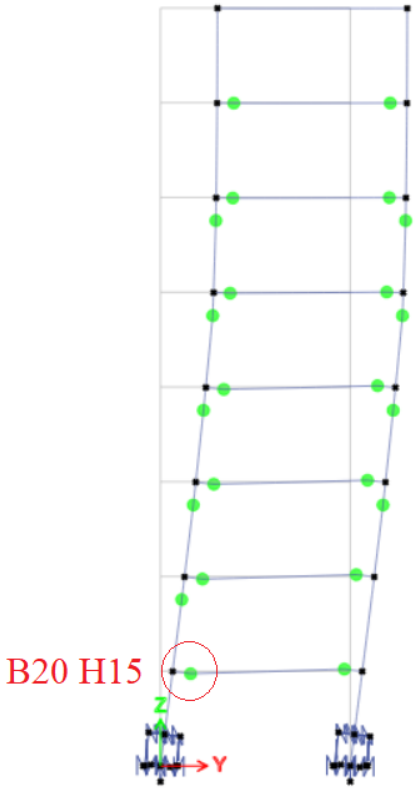

Figure 6.31: Hinge B20H15 results of Beam B20 were compared

The results for the two cases with different control parameters are given in Figures 6.32 and 6.33.

Models	$\theta_{plastic}/\theta_{yield}$
Model 1: α=0.005, c=0.5Fu	131.0147
Model 2: α=0.5, c=0.5Fu	264.6838
Model 3: α=1, c=0.5Fu	279.0882
Model 4: α=1.5, c=0.5Fu	283.5956
Model 5: α=2, c=0.5Fu	289.6691
Free Rocking Base	292.5809

Figure 6.32: Results for different α values,the c value is controlled

Models	$\theta_{plastic}/\theta_{yield}$
Model 6: α=1, c=0.25Fu	280.8382
Model 3: α=1, c=0.5Fu	279.0882
Model 7: α=1, c=0.75Fu	271.0221
Model 8: α=1, c=Fu	268.5882
Free Rocking Base	292.5809

Figure 6.33: Results for different c values,the α value is controlled

As can be seen from the plastic rotation over yield rotation ratios, as the alpha value is decreased, the damping is more effective which also indicates that the particle velocity is smaller than 1 m/s. And, as the damping coefficient increases while α is kept constant, the damping is more efficient, as expected. The FRB model's $\theta_{plastic}$ / θ_{yield} value for hinge B20H15 is higher than all of the damped cases, which shows that the damper is effective in reducing the permanent deformation of the structure.

For the fixed base case of the same model, both nonlinear fibers at story 1 column bases are past the ultimate capacity point. Whereas for the FRB model and the models equipped with dampers, none of the hinges reached ultimate capacity. The corresponding hinges on the fixed model at the end of the **3x Landers 3756** ground motion can be seen in Figure 6.34.

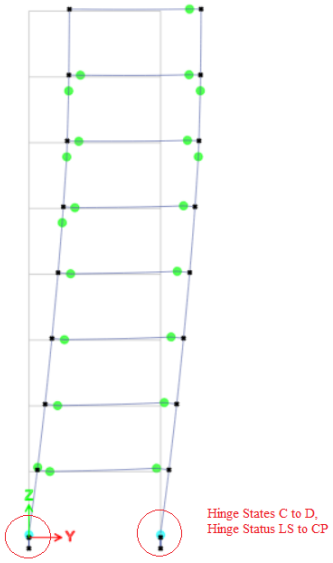

Figure 6.34: Fixed (Conventional) Model Hinging

6.5 Comparison of Fixed and PT Rocking Columns

As an alternative to the FRB models, post-tensioned rocking columns were modeled as well.

Initially, a single post-tensioning strand was added to the center of the rocking column, which showed very similar results to the FRB column system, the general responses for base shear and base moment were ranging 99-99.5% the same. Therefore, to improve the PT rocking column modeling, in 2D system, the modeling was revised and two unbonded post-tensioning strands were added near to the edges of the column section where the uplift is more effective and the restraining effect of the tendons can be better observed. This modeling approach is illustrated in Figure 6.35.

Figure 6.35: PT Rocking Base Model

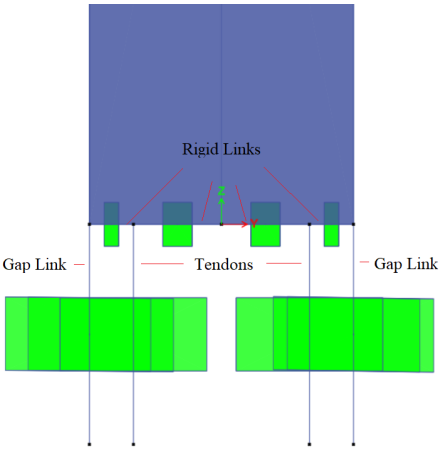

In order to save computational time and overcome the convergence issues, the analyses were conducted in 8 story 1 bay model.

For the post tensioned strands, two different parameters were considered in the analysis; the diameter of the post tensioning strands, d, and the post tensioning force, F_t. The rod diameters considered for this study were 15 mm and 30 mm. And the post tension force was applied as %10, %20, %30 and %40 of the ultimate tensile capacity of the post-tensioning strands. The analysis models are listed in Table 6.3.

Table 6.3: Comparison for Fixed and FRB+PT Rocking Base

Model	d (mm)	F_t
Model 1	15	$0.1F_{tu}$
Model 2	15	$0.2F_{tu}$
Model 3	15	$0.3F_{tu}$
Model 4	15	$0.4F_{tu}$
Model 5	30	$0.1F_{tu}$
Model 6	30	$0.2F_{tu}$
Model 7	30	$0.3F_{tu}$
Model 8	30	$0.4F_{tu}$

The values for the post-tensioning forces for each model are given in table 6.4

Table 6.4: Test Models for PT Rocking Base

d (mm)	**10% F_{ut} (kN)**	**20 % F_{ut} (kN)**	**30 % F_{ut} (kN)**	**40 % F_{ut} (kN)**
15	28.62	57.24	85.86	114.48
30	114.48	228.96	343.44	457.92

The load effect of the stressing of tendons were added to the system as a load case in ETABS environment, and the minor effect on strain on the tendons were ignored.
For the analysis to be successful, all the strands need to stay in the elastic range throughout the NTHA, which was ensured. The analysis was conducted under Landers 3756 time history case. The results that represent the general behavior, base shear ratios, are given in figures 6.36 and 6.37.

Models	Base Shear Ratio (Rocking/Fixed)
Model 1: drod=15 mm, Ft= 10 % Ftu	0.68784
Model 2: drod=15 mm, Ft= 20 % Ftu	0.68782
Model 3: drod=15 mm, Ft= 30 % Ftu	0.68673
Model 4: drod=15 mm, Ft= 40 % Ftu	0.68525
Free Rocking Base	0.68121

Figure 6.36: Results for models with d_{rod}=15 mm

Models	Base Shear Ratio (Rocking/Fixed)
Model 5: drod=30 mm, Ft= 10 % Ftu	0.72462
Model 6: drod=30 mm, Ft= 20 % Ftu	0.72288
Model 7: drod=30 mm, Ft= 30 % Ftu	0.70719
Model 8: drod=30 mm, Ft= 40 % Ftu	0.69959
Free Rocking Base	0.68121

Figure 6.37: Results for models with d_{rod}=30 mm

Despite the change in general results being small, it can be observed that as the rod diameter increases, the restraining effect of the tendons is larger, and the effectiveness of the rocking base is smaller, as expected. In addition, as the stressing force increases, the axial force applied on the first story columns increases since these columns are anchored. This improves the general behavior under NTHA since the direct weight over the rocking columns increases. This weight contributes to the re-centering of these columns.

6.6 Comparison of Fixed, FRB, PT-Rocking Base Models with and without Dampers

Finally, to see the effect of each examined case of FRB, FRB + Damper, PT-Rocking Base and PT-Rocking Base + Dampers cases on the benchmark model of 8 story 5 bay, and the extreme case of 8 story 1 bay. The comparison was carried out under Landers 3756 time history load case.

Model 1 case where α = 0.005, c=0.F_u was chosen for the damper property, and Model 5 case d_{rod}= 30 mm, F_t= 10 % F_{tu} was chosen for the tendon modeling.

The maximum base shear force and base moment results and respective ratios with

respect to the fixed base case of these five models under time history load case Landers 3756 can be seen in Figures 6.38 and 6.39 for the benchmark model (8 story 5 bay), and Figures 6.40 and 6.41 for the extreme case (8 story 1 bay) model.

	FY (kN)	MX (kN-m)
Fixed (Conventional) Base	-1085.62	89001.858
FRB	-979.895	88574.319
FRB + Dampers	-968.236	88988.684
PT Rocking Base	-992.062	95846.379
PT Rocking Base + Dampers	-977.432	88574.319

Figure 6.38: The base shear force and base moment results of the benchmark model

	(Rocking/Fixed)	
	Shear	**Moment**
FRB	0.6903	0.91446
FRB + Dampers	0.7382	0.93149
PT Rocking Base	0.7344	1.131114
PT Rocking Base + Dampers	0.7789	1.152639

Figure 6.39: The base shear force and base moment ratios with respect to fixed base (conventional) case for the benchmark model

	FY (kN)	MX (kN-m)
Fixed (Conventional) Base	-243.163	6785.9316
FRB	-167.86	6205.4831
FRB + Dampers	-179.503	6321.0139
PT Rocking Base	-178.59	7675.6643
PT Rocking Base + Dampers	-189.391	7821.7302

Figure 6.40: The base shear force and base moment results of the extreme model

	(Rocking/Fixed)	
	Shear	**Moment**
FRB	0.6903	0.91446
FRB + Dampers	0.7382	0.93149
PT Rocking Base	0.7344	1.131114
PT Rocking Base + Dampers	0.7789	1.152639

Figure 6.41: The base shear force and base moment ratios with respect to fixed base (conventional) case of the extreme model

As can be seen from the analysis results, although the differences between the rocking base models are small, the best performance is obtained with the FRB case compared to the PT Rocking base case. Furthermore, the dampers improve the response of the FRB and PT cases by reducing the nonlinear hinge responses, although the total base shear increases slightly (at most 1-2 % increase).

The story drifts, shears and displacement results were also plotted in Figures 6.42, 6.43, 6.44 and 6.45 for the benchmark model and in Figures 6.46, 6.47, 6.48 and 6.49 for the extreme case model. In these plots, the FRB and PT cases were compared to the fixed-based case separately. In the story drift plots it can be observed that at the lower story levels, the drifts are higher for the FRB and PT-Rocking base cases but after the second story level, the drifts are significantly reduced compared to the fixed base case. And with the addition of dampers, the story drifts are further reduced for both PT and FRB cases. In the shear and displacement plots, it can be seen that the FRB and PT Rocking Base cases both improve the base shear results with FRB slightly performing better. And in turn, the story displacements are slightly lower for the PT Rocking Base case compared to the FRB case as expected.
From the analysis results, it can also be observed that the reduction in story shears and drifts is much more significant for the extreme case of 8-story 1-bay compared to the benchmark model, 8-story 5-bay case.

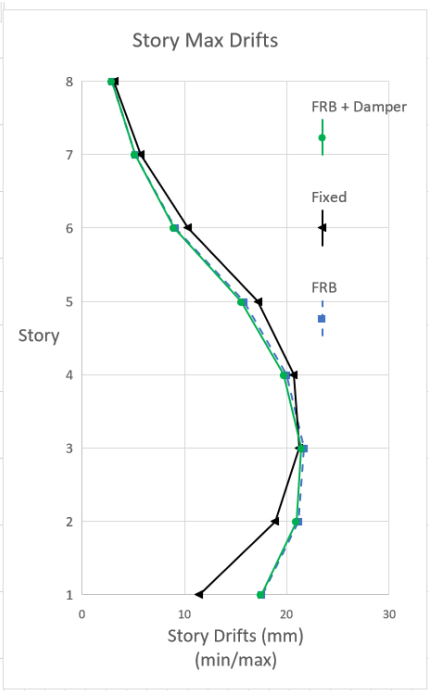

Figure 6.42: Maximum story drifts for Fixed, FRB and FRB + Dampers plotted for the benchmark model

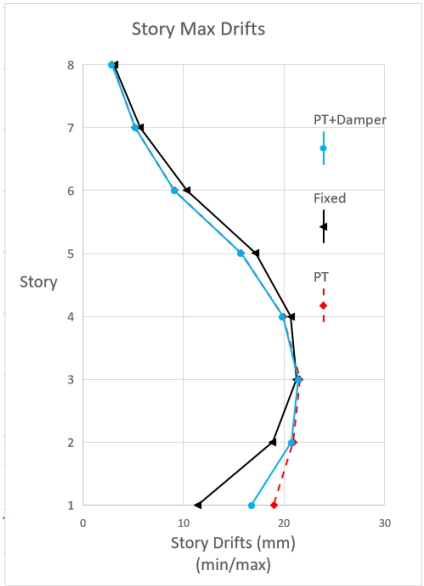

Figure 6.43: Maximum story drifts for Fixed, PT and PT + Dampers plotted for the benchmark model

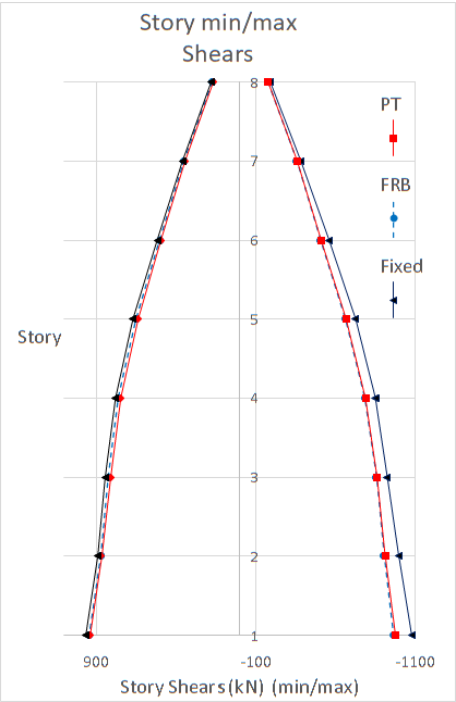

Figure 6.44: Story min/max shears for Fixed, PT, and FRB plotted for the benchmark model

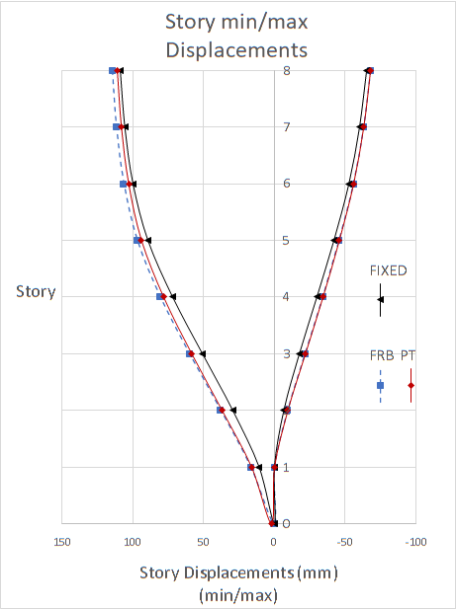

Figure 6.45: Story min/max displacements for Fixed, PT, and FRB plotted for the benchmark model

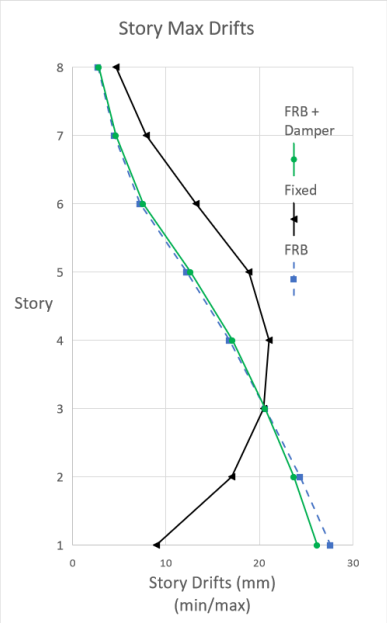

Figure 6.46: Maximum story drifts for Fixed, FRB and FRB + Dampers plotted for the extreme case

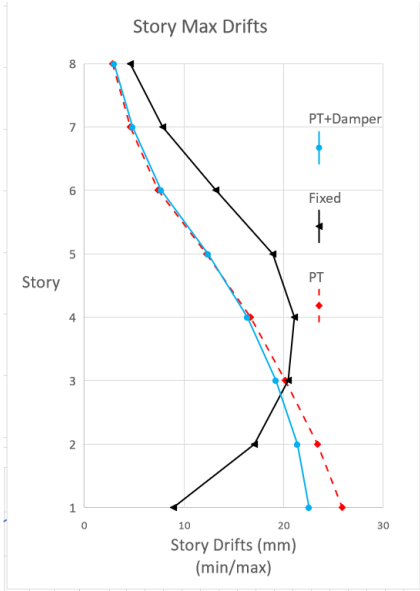

Figure 6.47: Maximum story drifts for Fixed, PT and PT + Dampers plotted for the extreme case

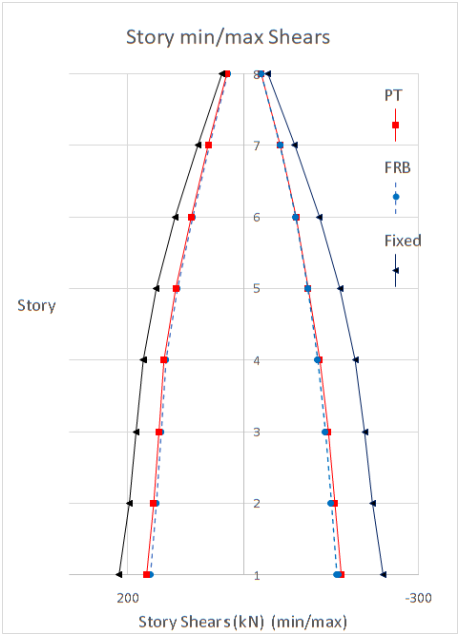

Figure 6.48: Story min/max shears for Fixed, PT, and FRB plotted for the extreme case

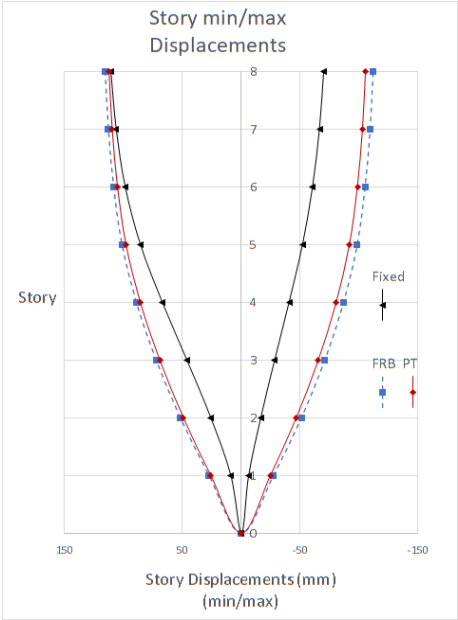

Figure 6.49: Story min/max displacements for Fixed, PT, and FRB plotted for the extreme case

CHAPTER 7

CONCLUSIONS

The main purpose of this study was to investigate the effectiveness of rocking outer columns on seismic performance. In doing so, multiple different parameters were also accounted for and presented with a comprehensive set of tests. The analyses were conducted by simplifying the 3D models by taking a strip in the YZ plane and narrowing down the active degrees of freedom to the 2D YZ plane; Uy, Uz, and Rx. This way, it was ensured that the analysis time is optimal and the effects of the uplift can be observed. Different parameters considered in this study are:

- 2D Frame with/without shear walls.
- Different number of stories (4, 8, 12 and 16).
- Different number of bays (1, 2, 3, 4 and 5).
- Modeling of the rocking base
  - Free Rocking Base (FRB)
  - Post-tensioned rocking base (PT Rocking Base)
    - Different tensioning forces for PT strands.
    - Different rod diameters for PT strands.
- Addition of dampers
  - Different damping exponent, α values for damper design.
  - Different damping coefficient, c, values for damper design.
- Different ground motion intensity levels (0.25g, 0.5g, 0.75g, 1g).

In this study, the rocking response is found to be a very effective way for energy absorption with up to %11 reductions in base shear for FRB + Dampers case for the benchmark model and with even higher performance for the lower number of stories and bays. The parametric study shows that this method is most effective in low-rise buildings with a lesser number of bays performing best at 4 story 1 bay model with % 33 percent reduction in base shear.

The initial comparison of the shear-walled model (AA-Plane) and the model without shear walls (BB-Plane) models showed that the shear-walled frame does not perform as well as the model without shear walls even in higher ground motion intensity levels where the effect of rocking is better observed. The most efficient method for energy absorption found in this study proved to be FRB systems equipped with viscous fluid dampers. The PT Rocking base models also perform quite well with only a 1-2 % difference compared to the FRB models. The controlled increase in the post-tensioning force improves the behavior due to its contribution to re-centering during ground shaking.

The addition of vertical fluid viscous dampers to both FRB and PT Rocking Base models increased the general response slightly (1-2 % increase in base shear) due to the additional restraint these provide against rocking. But had significant effects at the element level with notably lower plastic hinge rotation values.

REFERENCES

[1] N. Makris, "A half-century of rocking isolation," *Earthquake and Structures*, vol. 7, no. 6, pp. 1187–1221, 2014.

[2] J. B. Mander, M. J. N. Priestley, and R. Park, "Theoretical stress-strain model for confined concrete," *Journal of Structural Engineering*, vol. 114, pp. 1804–1826, 9 1988.

[3] G. Ríos-García and A. Benavent-Climent, "New rocking column with control of negative stiffness displacement range and its application to RC frames," *Engineering Structures*, vol. 206, 2020.

[4] C. T. Cheng and C. H. Chao, "Seismic behavior of rocking base-isolated structures," *Engineering Structures*, vol. 139, 2017.

[5] Y. Chen, C. Chen, Z. Xu, and W. Yu, "Seismic performance study on prefabricated self-centering rocking steel frame," *Jianzhu Jiegou Xuebao/Journal of Building Structures*, vol. 42, pp. 23–34, 2021.

[6] Z. Zhao and X. Su, "Seismic response analysis of prestressed concrete rocking frame," *Applied Sciences (Switzerland)*, vol. 11, no. 2, pp. 1–27, 2021.

[7] G. W. Housner, "The behavior of inverted pendulum structures during earthquakes," *Bulletin of the Seismological Society of America*, vol. 53, pp. 403–417, 1963.

[8] M. Midorikawa, T. Azuhata, T. Ishihara, Y. Matsuba, Y. Matsushima, and A. Wada, "Earthquake response reduction of buildings by rocking structural systems," in *Smart Structures and Materials 2002: Smart Systems for Bridges, Structures, and Highways*, vol. 4696, pp. 265–272, SPIE, jun 2002.

[9] T. C. Steele and L. D. Wiebe, "Dynamic and equivalent static procedures for capacity design of controlled rocking steel braced frames," *Earthquake Engineering and Structural Dynamics*, vol. 45, pp. 2349–2369, nov 2016.

[10] Y. W. Li, G. Q. Li, J. Jiang, and Y. B. Wang, "Experimental study on seismic performance of RC frames with Energy-Dissipative Rocking Column system," *Engineering Structures*, vol. 194, pp. 406–419, 2019.

[11] H. Roh and A. M. Reinhorn, "Modeling and seismic response of structures with concrete rocking columns and viscous dampers," *Engineering Structures*, vol. 32, no. 8, pp. 2096–2107, 2010.

[12] F. Prieto and P. B. Lourenço, "On the rocking behavior of rigid objects," *Meccanica*, vol. 40, 2005.

[13] D. Kalliontzis and S. Sritharan, "Dynamic response and impact energy loss in controlled rocking members," *Earthquake Engineering and Structural Dynamics*, vol. 49, 2020.

[14] S. G. Abd-Elhamid, R. M. G. E. El-Tahawy, and M. N. E.-D. Fayed, "Dynamic behavior of multi-story concrete buildings based on non-linear pushover time history analyses," *Advances in Science, Technology and Engineering Systems*, vol. 5, 2020.

[15] M. Dicleli and C. Durucan, "Evaluation of displacement coefficient method for seismically retrofitted buildings with various ductility capacities," *Earthquake Engineering and Structural Dynamics*, vol. 43, 2014.

[16] B. M.Das, "Principles of foundation engineering," *McGraw-Hill handbooks*, 2002.

[17] S. Acikgoz and M. J. Dejong, "The interaction of elasticity and rocking in flexible structures allowed to uplift," *Earthquake Engineering and Structural Dynamics*, vol. 41, no. 15, pp. 2177–2194, 2012.

[18] T. Azuhata, T. Ishihara, M. Midorikawa, and A. Wada, "Seismic response reduction of steel frames with multi-spans by applying rocking structural system," in *Proceedings of the 5th International Conference on Behaviour of Steel Structures in Seismic Areas - Stessa 2006*, pp. 659–664, 2006.

[19] S. Acikgoz and M. J. Dejong, "The interaction of elasticity and rocking in flexible structures allowed to uplift," *Earthquake Engineering and Structural Dynamics*, vol. 41, no. 15, pp. 2177–2194, 2012.

[20] S. A. Anagnostopoulos, "Pounding of buildings in series during earthquakes," *Earthquake Engineering Structural Dynamics*, vol. 16, 1988.

[21] M. N. Chatzis and A. W. Smyth, "Robust Modeling of the Rocking Problem," *Journal of Engineering Mechanics*, vol. 138, no. 3, pp. 247–262, 2012.

[22] A. K. Chopra and S. C. Yim, "Simplified Earthquake Analysis of Structures with Foundation Uplift," *Journal of Structural Engineering*, vol. 111, no. 4, pp. 906–930, 1985.

[23] M. Midorikawa, T. Azuhata, T. Ishihara, A. Wada, and I. Okawa, "FEM Analuses on Seismic Responses of Rocking Structural Systems with Tielding Base Plates," *Statewide Agricultural Land Use Baseline 2015*, vol. 1, 2015.

[24] A. Rutenberg, P. C. Jennings, and G. W. Housner, "The response of veterans hospital building 41 in the San Fernando earthquake," *Earthquake Engineering Structural Dynamics*, vol. 10, no. 3, pp. 359–379, 1982.

[25] R. DesRoches and S. Muthukumar, "Implications of seismic pounding on the longitudinal response of multi-span bridges - an analytical perspective," *Earthquake Engineering and Engineering Vibration*, vol. 3, 2004.

[26] L. Lu, L. Jiang, H. Li, and X. L. Lü, "Shaking table tests for aseismic performance of a controllable rocking reinforced concrete frame with column-end-hinge joints," *Zhendong yu Chongji/Journal of Vibration and Shock*, vol. 35, feb 2016.

[27] L. Lu, X. Liu, J. Chen, and X. Lu, "Seismic performance of a controlled rocking reinforced concrete frame," *Advances in Structural Engineering*, vol. 20, pp. 4–17, jan 2017.

[28] N. Reggiani Manzo and M. F. Vassiliou, "Displacement-based analysis and design of rocking structures," *Earthquake Engineering and Structural Dynamics*, vol. 48, no. 14, pp. 1613–1629, 2019.

[29] J. J. Ajrab, G. Pekcan, and J. B. Mander, "Rocking wall–frame structures with supplemental tendon systems," *Journal of Structural Engineering*, vol. 130, pp. 895–903, 2004.

[30] M. Aghagholizadeh and N. Makris, "Earthquake response analysis of yielding structures coupled with vertically restrained rocking walls," *Earthquake Engineering and Structural Dynamics*, vol. 47, pp. 2965–2984, 2018.

[31] T. Azuhata and T. Ishihara, "A simpified prediction method for seismic responses of building frame structures allowed to uplift," vol. 2, pp. 2950–2962, 2017.

[32] J. A. Bachmann, M. F. Vassiliou, M. Broccardo, B. Stojadinovic, and M. Strand, "Modelling of rocking structures: Are our models good enough?," 2019.

[33] J. L. Beck and R. I. Skinner, "The seismic response of a reinforced concrete bridge pier designed to step," *Earthquake Engineering Structural Dynamics*, vol. 2, pp. 343–358, 1973.

[34] J. Binder and C. Christopoulos, "Seismic performance of hybrid ductile-rocking braced frame system," *Earthquake Engineering and Structural Dynamics*, vol. 47, pp. 1394–1415, 2018.

[35] H. V. Burton, G. G. Deierlein, D. Mar, K. M. Mosalam, J. Rodgers, and S. Günay, "Rocking spine for enhanced seismic performance of reinforced concrete frames with infills," *Journal of Structural Engineering*, vol. 142, 2016.

[36] E. Dimitrakopoulos, M. Dejong, and A. I. Giouvanidis, "Seismic assessment of rocking bridge bents using an equivalent rocking block," pp. 1–8, 2013.

[37] T. C. Steele and L. D. Wiebe, "Collapse risk of controlled rocking steel braced frames with different post-tensioning and energy dissipation designs," *Earthquake Engineering and Structural Dynamics*, vol. 46, pp. 2063–2082, 10 2017.

[38] M. Pollino, "Structural and non-structural seismic demands on controlled rocking steel braced frame buildings," pp. 1541–1552, 2012.

[39] T. Takeuchi, X. Chen, and R. Matsui, "Seismic performance of controlled spine frames with energy-dissipating members," *Journal of Constructional Steel Research*, vol. 114, pp. 51–65, 7 2015.

[40] T. Ther and L. P. Kollár, "Refinement of housner's model on rocking blocks," *Bulletin of Earthquake Engineering*, vol. 15, pp. 2305–2319, 2017.

[41] Y. Li and G. Li, "Mechanism and application of dual energy-dissipative rocking columns in rc frames for seismic mitigation," *Jianzhu Jiegou Xuebao/Journal of Building Structures*, vol. 42, pp. 65–75, 2021.

[42] E. Yooprasertchai and P. Warnitchai, "Seismic performance of precast hybrid moment-resisting frame/rocking wall systems," *Magazine of Concrete Research*, vol. 70, pp. 1118–1134, 2018.

[43] M. Midorikawa, T. Azuhata, T. Ishihara, and A. Wada, "Shaking table tests on seismic response of steel braced frames with column uplift," *Earthquake Engineering and Structural Dynamics*, vol. 35, pp. 1767–1785, 2006.

[44] S. Al-Subaihawi and S. Pessiki, "Static pushover response of spring anchored unbonded post-tensioned rocking systems," *Engineering Structures*, vol. 200, 2019.